

How important are fluctuations in the treatment of internal friction in polymers?

R. Kailasham,^{1,2,3} Rajarshi Chakrabarti^{*,2,a)} and J. Ravi Prakash^{*3,b)}

¹⁾*IITB-Monash Research Academy, Indian Institute of Technology Bombay, Mumbai, Maharashtra - 400076, India*

²⁾*Department of Chemistry, Indian Institute of Technology Bombay, Mumbai, Maharashtra - 400076, India*

³⁾*Department of Chemical Engineering, Monash University, Melbourne, VIC 3800, Australia*

The Rouse model with internal friction (RIF), a widely used theoretical framework to interpret the effects of internal friction on conformational transitions in biomolecules, is shown to be an approximate treatment that is based on preaveraging internal friction. By comparison with Brownian dynamics simulations of an exact coarse-grained model that incorporates fluctuations in internal friction, the accuracy of the preaveraged model predictions is examined both at and away from equilibrium. While the two models predict intrachain autocorrelations that approach each other for long enough chain segments, they differ in their predictions for shorter segments. Furthermore, the two models differ qualitatively in their predictions for the chain extension and viscosity in shear flow, which is taken to represent a prototypical out-of-equilibrium condition.

Macromolecules in solution experience an additional mode of dissipation or friction due to intramolecular interactions, over and above the solvent drag, which resists their conformational reconfiguration¹⁻⁶. This additional mode of dissipation termed as *internal friction* or *internal viscosity*⁷⁻¹² (IV), has been known to significantly affect the conformational dynamics¹³⁻¹⁹ of chains and the rheology²⁰⁻²² of polymer solutions. In force-spectroscopic measurements on polysaccharides or condensed DNA²³⁻²⁶, the dissipation associated with stretching the molecules is much greater than that can be attributed to solvent friction alone. An important class of intramolecular chemical reactions²⁷ relies on the formation of a loop between distant segments of a polymer chain, and internal friction has been shown to affect the looping and reconfiguration times in polymer molecules^{11,12,18,28}. The most widely used theoretical framework for the interpretation of internal friction effects^{17,29-31} is the Rouse model with internal friction³² (RIF) and its variants^{11,12,28}, which modify the standard continuum Rouse model to include an additional frictional force that resists changes in the curvature of the space-curve representing the polymer molecule. While these models remain preferred due to their analytical tractability, their accuracy, from a theoretical standpoint, has so far been unquestioned. We first show that the RIF model represents an approximation that ignores fluctuations in the internal friction force and is rather a preaveraged treatment. We have recently developed an exact numerical solution to the Rouse model with fluctuating internal friction [Ref. 33, under review], and used it to estimate linear-viscoelastic and steady-shear viscometric functions using Brownian dynamics (BD) simulations. In this paper, the exact model is used to test the accu-

racy of the RIF model, by comparing their predictions for quantities both at and away from equilibrium.

The effect of internal friction on the dynamics of protein reconfiguration is commonly quantified experimentally by tagging the molecule with fluorescent donor-acceptor pairs along their contour length, and extracting a characteristic reconfiguration time from the autocorrelation of the fluorescence signal^{18,31}. Analytical and simulation estimates of the reconfiguration time are based on the autocorrelation of the vector that connects the tagged monomers along the chain^{11,12,28}. We examine this property, which represents an equilibrium situation, where the molecule is suspended in a quiescent fluid. In order to examine the importance of fluctuations away from equilibrium, a polymer molecule subjected to simple shear flow is considered as a prototypical out-of-equilibrium process. Several biological processes, such as ciliary and flagellar oscillations in microorganisms³⁴⁻³⁶, are driven by the hydrolysis of ATP molecules, and the contribution from internal friction in these far-from-equilibrium processes is seen to outweigh hydrodynamic drag by nearly an order of magnitude. Protein molecules such as hormones and antibodies are commonly subjected to shear flow during various stages of bioprocessing³⁷. The conformational dynamics of these molecules in flow directly affects their structure and function, which further adds relevance to the study of the dynamic response of polymers to shear flow.

We find that the equilibrium predictions made by the preaveraged model and the one with fluctuations differ at small separations between the tagged monomers along the polymer backbone, with the difference diminishing with an increase in the inter-tag separation. However, in the presence of shear flow, the two model predictions differ starkly and qualitatively: the preaveraged model predicts values for the chain extension and viscosity that are identical to the standard Rouse model, with the internal friction parameter only affecting the transient phase that precedes the attainment of steady state. Contrarily,

^{a)}Electronic mail: rajarshi@chem.iitb.ac.in

^{b)}Electronic mail: ravi.jagadeeshan@monash.edu

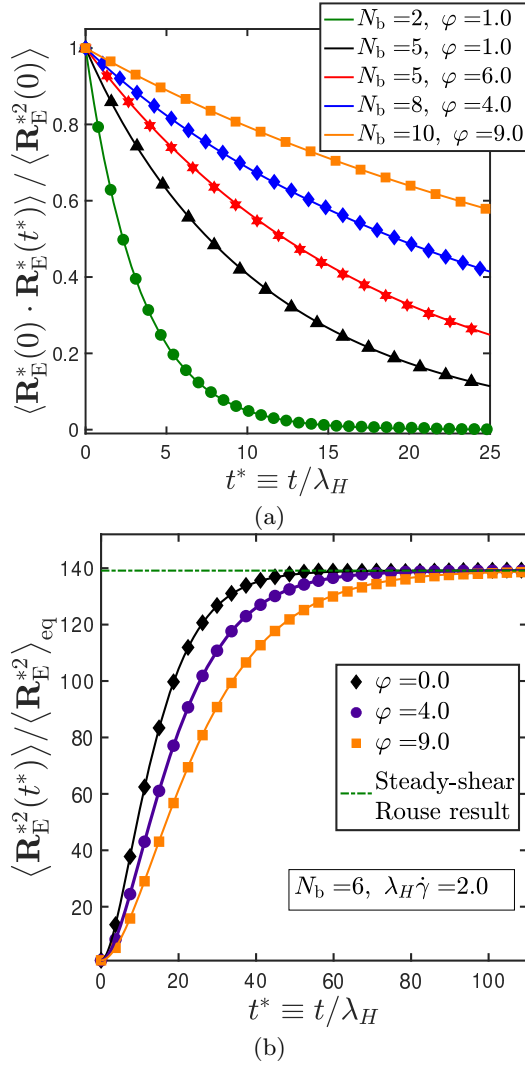


FIG. 1. BD simulation results of the preaveraged internal friction model, for: (a) Normalized autocorrelation of the end-to-end vector at equilibrium, and (b) transient evolution of the mean-squared end-to-end vector in shear flow, obtained by numerically integrating Eq. (22). The lines in (a) and (b) represent discrete RIF results given by Eq. (18) and Eq. (19), respectively. Error bars, which represent standard error of the mean, are roughly of the same size or smaller than the symbols used.

exact BD simulations which account for fluctuations in IV establish that both the transients and the steady-state values are modified by internal friction³³.

The standard RIF model is in the continuous chain limit, but it is convenient to work with a discrete model for ease of comparison with simulations. As shown in Figures S2 and S3 of the Supplementary Material, the discrete model is identical to the continuous chain RIF model as the number of beads, $N_b \gg 1$. In the discrete RIF model, the beads, each of radius a and suspended in a solvent of viscosity η_s , are located at positions $\{\mathbf{r}_1, \mathbf{r}_2, \dots, \mathbf{r}_{N_b}\}$, and connected by Hookean springs of

stiffness H in parallel with dashpots that have a damping coefficient $(K/3)$. The factor of 3 is explained below. The dashpots provide a resistive force that is proportional to the relative velocity between adjacent beads, and the force due to internal friction on a bead μ not at the chain ends is given by

$$\begin{aligned} \mathbf{F}_\mu^{(\text{IV}),\text{RIF}} &= (K/3)(\dot{\mathbf{r}}_{\mu+1} - \dot{\mathbf{r}}_\mu) - (K/3)(\dot{\mathbf{r}}_\mu - \dot{\mathbf{r}}_{\mu-1}) \\ &= (K/3)[\dot{\mathbf{r}}_{\mu+1} - 2\dot{\mathbf{r}}_\mu - \dot{\mathbf{r}}_{\mu-1}] \end{aligned} \quad (1)$$

where $\dot{\mathbf{r}}_\mu = d\mathbf{r}_\mu/dt$. The overdamped Langevin equation for the time evolution of \mathbf{r}_μ , is given as

$$\frac{d\mathbf{r}_\mu}{dt} = -\left(\frac{H}{\zeta} + \frac{K}{3\zeta} \frac{d}{dt}\right) \sum_{\nu=1}^{N_b} A_{\mu\nu}^{(\text{R})} \mathbf{r}_\nu + \boldsymbol{\kappa} \cdot \mathbf{r}_\mu + \boldsymbol{\xi}_\mu(t) \quad (2)$$

where $\zeta = 6\pi\eta_s a$ is the bead friction coefficient, $A_{\mu\nu}^{(\text{R})}$ are elements of the Rouse matrix⁷, and $\boldsymbol{\kappa}$ represents the flow-field, which is $\mathbf{0}$ in the absence of flow, and

$$\boldsymbol{\kappa} = \begin{pmatrix} 0 & \dot{\gamma} & 0 \\ 0 & 0 & 0 \\ 0 & 0 & 0 \end{pmatrix} \quad (3)$$

for simple shear flow, where $\dot{\gamma}$ denotes the shear rate. The characteristic length- and time-scales in the coarse-grained models discussed above are defined to be $l_H = \sqrt{k_B T/H}$ and $\lambda_H = \zeta/4H$, respectively, where k_B is Boltzmann's constant and T the absolute temperature. Scaled dimensionless variables are denoted with an asterisk as superscript. The internal friction parameter, $\varphi \equiv K/\zeta$, is taken to be the ratio of the damping coefficient of the dashpot to the bead friction coefficient. The moments of the noise term, $\boldsymbol{\xi}_\mu(t)$, are not specified in real space, but rather in normal-mode space. Essentially, eq. (2) is solved (see section 'Analytical solutions' in the Methods section) by first using the eigenvectors, $a_p = 4 \sin^2(p\pi/2N_b)$; $p \in [0, (N_b - 1)]$, of the Rouse matrix for projecting the bead positions into normal-mode space, followed by the assumption that the noise term in normal mode space is white, so as to satisfy the requirements of equipartition. This treatment results in a solution which is similar to the standard Rouse model, with a renormalization of the mode relaxation times. The expression for the normalized dimensionless autocorrelation of the end-to-end vector, $\mathbf{R}_E^* = \mathbf{r}_{N_b}^* - \mathbf{r}_1^*$, for the discrete RIF model at equilibrium ($\boldsymbol{\kappa} = \mathbf{0}$) is derived to be

$$\begin{aligned} \frac{\langle \mathbf{R}_E^*(0) \cdot \mathbf{R}_E^*(t^*) \rangle}{\langle \mathbf{R}_E^2(0) \rangle} &= \left[\frac{8}{N_b(N_b - 1)} \right] \sum_{p:\text{odd}}^{N_b-1} \cos^2\left(\frac{p\pi}{2N_b}\right) \\ &\quad \times \left(\frac{1}{a_p}\right) \exp\left[-\left(\frac{3a_p}{3 + \varphi a_p}\right) \frac{t^*}{4}\right] \end{aligned} \quad (4)$$

A solution for the continuum RIF chain subjected to shear flow is not available in the literature. We have

derived an expression for the transient evolution of the dimensionless mean-squared end-to-end vector in shear flow scaled by its equilibrium value, $\langle \mathbf{R}_E^{*2}(t^*) \rangle / \langle \mathbf{R}_E^{*2} \rangle_{\text{eq}}$, as detailed in Sec. II B of the Supplementary Material.

We show next that a Rouse model with preaveraged internal friction, constructed using the principles of polymer kinetic theory^{7,38} (PKT), is formally identical to the RIF model. A Hookean bead-spring-dashpot chain is considered, similar to the RIF model, except the dashpot coefficient is taken to be K . The total force on a bead μ (not at the chain ends) due to internal viscosity is given by⁸

$$\begin{aligned} \mathbf{F}_\mu^{(\text{IV})} = & K \left(\frac{\mathbf{Q}_\mu \mathbf{Q}_\mu}{Q_\mu^2} \right) \cdot \llbracket \dot{\mathbf{r}}_{\mu+1} - \dot{\mathbf{r}}_\mu \rrbracket \\ & - K \left(\frac{\mathbf{Q}_{\mu-1} \mathbf{Q}_{\mu-1}}{Q_{\mu-1}^2} \right) \cdot \llbracket \dot{\mathbf{r}}_\mu - \dot{\mathbf{r}}_{\mu-1} \rrbracket \end{aligned} \quad (5)$$

where $\mathbf{Q}_\mu \equiv \mathbf{r}_{\mu+1} - \mathbf{r}_\mu$ is the connector vector joining the μ^{th} and the $(\mu+1)^{\text{th}}$ bead, and $\llbracket \cdot \rrbracket$ represents an average over the distribution of velocities in the phase space. The equilibrium configurational distribution function for the model is unaltered by the presence of internal viscosity, and is simply given by the Gaussian distribution function for a Rouse chain. The preaveraging approximation entails a replacement of the underlined projection operators in Eq. (5) by their average taken with respect to the equilibrium distribution function, which may be evaluated to be $(\delta/3)$ ³⁹. The resultant internal friction force is then

$$\mathbf{F}_\mu^{(\text{IV}),\text{preav.}} = \left(\frac{K}{3} \right) \llbracket \dot{\mathbf{r}}_{\mu+1} - 2\dot{\mathbf{r}}_\mu - \dot{\mathbf{r}}_{\mu-1} \rrbracket \quad (6)$$

which is identical to the RIF description of the same force as given by Eq. (1). The governing stochastic differential equation for the preaveraged IV model is numerically integrated using BD simulations (see section ‘Preaveraged internal viscosity model’ in the Methods section). Notably, the use of the preaveraging approximation as a means to make flexible polymer models with internal friction analytically tractable was also suggested by Fixman⁴⁰ several decades ago.

In Fig. 1, simulation results at equilibrium and in shear flow, obtained by numerically integrating the stochastic differential equation for the preaveraged IV model using BD simulations (shown as symbols) have been compared against discrete RIF predictions (indicated by lines), for several parameter values. The excellent agreement between the two model predictions establishes their equivalence. Furthermore, the preaveraged treatment predicts that internal friction only affects the time-evolution of the mean-squared end-to-end vector in shear flow, but not its steady-state value which is identical to the standard Rouse model prediction.

As the next step, the accuracy of the preaveraging approximation is compared against the exact numerical solution³³ we have derived recently, in which the original

non-preaveraged form of the internal friction force given by Eq. (5) is used.

In Fig. 2, the normalized autocorrelation of $\mathbf{R}_{\mu\nu}^* \equiv \mathbf{r}_\nu^* - \mathbf{r}_\mu^*$ in a chain with N_b beads predicted by the discrete RIF model (indicated by lines) is compared against exact BD simulation results of a model with fluctuating internal friction (shown as symbols). The notation $\{\mu, \nu, N_b\}$ uniquely identifies the vector originating at the bead index μ and terminating at ν in a chain of N_b beads. The parameter space specified by $\{\mu, \nu, N_b\}$ may broadly be classified into three topological classes^{11,41–43}, and these categories have been considered in Fig. 2 (a)–(c). In Fig. 2 (a), the end-to-end case is considered, where μ and ν are taken to be the terminal beads in a chain. Fig. 2 (b) represents the end-to-interior topology class, where ν is taken to be a terminal bead, and μ is chosen from the interior set of beads, while Fig. 2 (c) represents the interior-to-interior case wherein both μ and ν are taken to be interior beads. In all the three cases, the difference between the fluctuating IV model and the preaveraged one is seen to diminish with an increase in $\nu - \mu$, i.e., the number of beads between the μ and ν positions. A similar qualitative trend was observed for other values of φ , and consequently, $\varphi = 3.0$, has been used for all the cases considered in Fig. 2. In Fig. 2 (d), the root-mean-squared difference (RMSD, Δ) between the two model results are plotted against the bead number μ , at two different values of the interbead separation, $\nu - \mu$. It is observed that the RMSD decreases with an increase in the interbead separation, and is fairly insensitive to the specific choice of the bead number μ . This implies that the end-to-interior, and the interior-to-interior topology classes may be considered equivalent with regards to the measured deviation between the preaveraged and fluctuating IV results.

There are two implications to the trend observed in Fig. 2: firstly, the preaveraged model is sufficiently accurate for characterizing the bead connector vector correlations of longer segments, as compared to local correlations corresponding to shorter chain segments, and secondly, the preaveraged model may satisfactorily be used for end-to-end vector reconfiguration time calculations provided that a sufficiently fine enough level of discretization (i.e., large enough N_b) is chosen. Note, however, that the choice of N_b is not arbitrary, and its largest permitted value is the number of Kuhn segments in the underlying polymer molecule. For example, the preaveraged IV model^{12,18,31} has been used for studying internal friction effects in the sixty-seven amino-acid residue cold shock protein at various concentrations of the denaturant, guanidinium chloride (GdmCl). The protein has a Kuhn segment length of about five residues at 6M GdmCl, which implies that the number of Kuhn segments in the molecule, and consequently the finest level of discretization, N_b , is $(67/5) \approx 13$. From Fig. 2, it would appear that at such values of N_b , the use of the preaveraged IV model for the calculation of the reconfiguration time would be justified for an internal friction

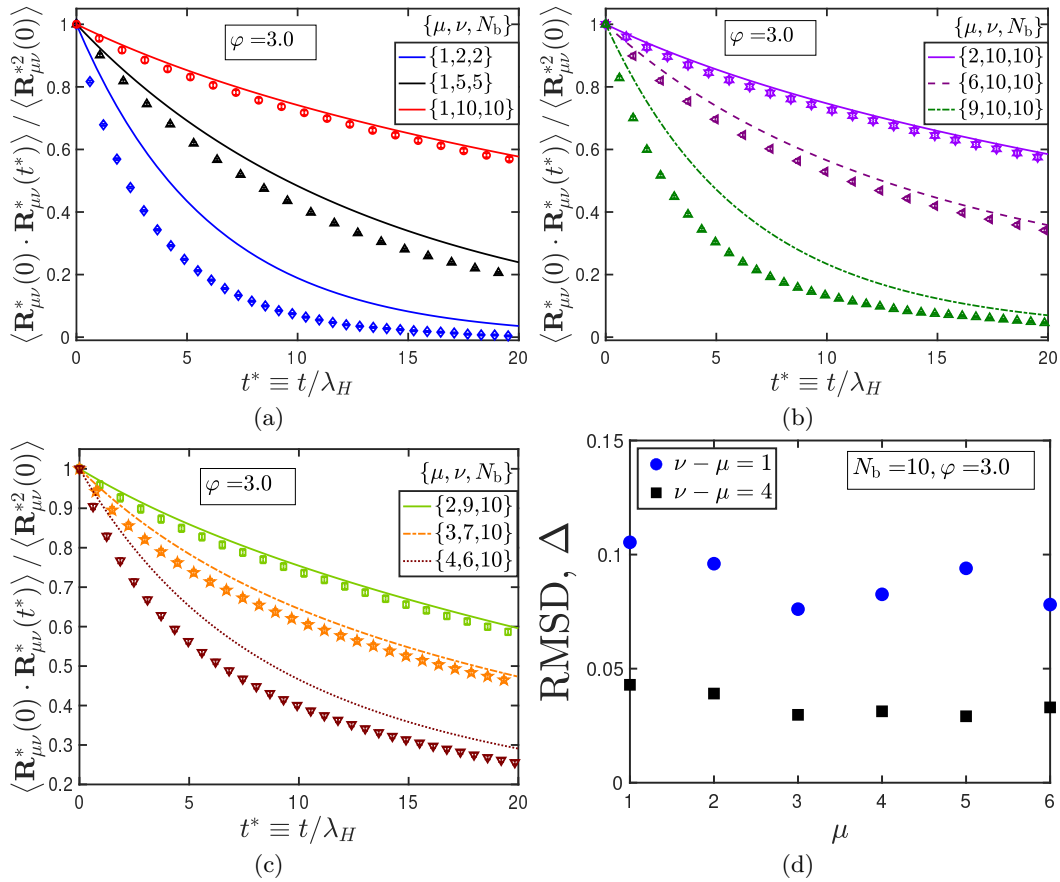


FIG. 2. Normalized autocorrelation of $\mathbf{R}_{\mu\nu}^*$, the vector connecting the μ^{th} and ν^{th} bead in a chain with N_b beads, for (a) end-to-end, (b) end-to-interior, and (c) interior-to-interior cases. The notation $\{\mu, \nu, N_b\}$ is used to completely specify the vector originating at the bead index μ and terminating at ν in a chain with N_b beads. Lines represent preaveraged model results. Symbols are BD simulation results on the Rouse model with fluctuating internal friction. An internal friction parameter of $\varphi = 3.0$ has been used for all the cases. Subfigure (d) represents the root-mean-squared difference between the two model results (see section ‘Analytical solutions’ in the Methods section for the definition of Δ) for various values of the interbead separation $\nu - \mu$.

parameter of $\varphi = 3.0$. The discrepancy between the two model predictions, however, is expected to increase with the internal friction parameter. Furthermore, internal friction has also been observed in a synthetic tryptophan cage molecule^{13,44} with twenty-residues, whose Kuhn segment length has not been reported, and it would appear that fluctuations in internal friction should be included for modeling such small molecules, given the constraint on the level of discretization.

In Fig. 3, the normalized, steady-state mean-squared end-to-end distance of a chain in simple shear flow is plotted as a function of the dimensionless shear rate. The lines, which represent the preaveraged model results, coincide with the simple Rouse model predictions implying that the steady-shear values are unaffected by the internal friction parameter, as also evident from Fig. (1) (b). The model with fluctuating internal friction, however, predicts that the extension in shear-flow is a function of the internal friction parameter.

There exist no prior studies of the viscometric functions predicted by the Rouse model with preaveraged internal friction. We have derived an expression for the stress tensor by using the Giesekus formula⁷ [see Eqs. (24)-(26) in the Methods section], since this choice has been shown to lead to thermodynamically consistent results for models with fluctuating IV⁴⁵. An important rheological consequence of internal friction is the appearance of a discontinuous, shear-rate-independent, jump in viscosity at the inception of flow^{5,20,46}. This phenomenon, called ‘‘stress jump’’ is not predicted by other bead-spring-chain models. In Fig. 4, the stress jumps predicted by the preaveraged and the fluctuating IV models are plotted as a function of the chain lengths and the internal friction parameter. A semi-analytical approximation for the stress jump in Rouse chains with fluctuating IV has been derived by Manke and Williams²⁰, and compares excellently against exact BD simulation results³³, with the accuracy of the approximation observed to im-

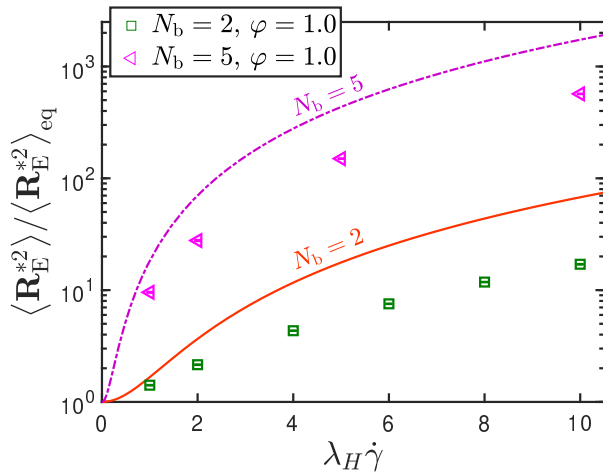


FIG. 3. Normalized steady-state mean-squared distance as a function of dimensionless shear rate for chains in shear flow. Lines correspond to preaveraged model results given by Eq. (20). Symbols are BD simulation results on the Rouse model with fluctuating internal friction.

prove with an increase in the number of beads. This approximate solution has therefore been used to plot Fig. 4 (b). From Figs. 4 (a) and 4 (b), it is observed that while the fluctuating IV model predicts that the stress jump scales linearly with the chain length for values of the internal friction parameter spanning two orders of magnitude, a similar linear dependence in the preaveraged model predictions is pushed to larger values of the number of springs, N , as the internal friction parameter is increased. From Fig. 4 (c), it is observed that for a given value of the internal friction parameter, φ , and chain length, the stress jump predicted by the fluctuating IV model is lower than that predicted by the preaveraged model. Furthermore, for a given value of the chain length, the stress jump predicted by the fluctuating IV model saturates with an increase in the internal friction parameter. No such saturation, however, is predicted by the preaveraged IV model.

In Fig. 5, the transient evolution of shear-viscosity for models with preaveraged and fluctuating IV are compared for a five-bead chain. As seen from Fig. 5 (a), at a fixed value of the shear rate, there is a qualitative difference in the transient evolution of viscosity as predicted by the two models for two different values of the internal friction parameter. In Fig. 5 (b), the transient response is plotted for a fixed value of the internal friction parameter and two different shear rates. The preaveraged model prediction is independent of the shear rate, and grows monotonously, while the viscosity predicted by the model with fluctuations is shear-rate-dependent, going through a local maximum for larger shear rates, as seen clearly for the $\lambda_H \dot{\gamma} = 20.0$ case.

Furthermore, in the long-time limit, the preaveraged IV model predicts a shear-rate independent, constant value of the viscosity, equal to the Rouse viscosity for

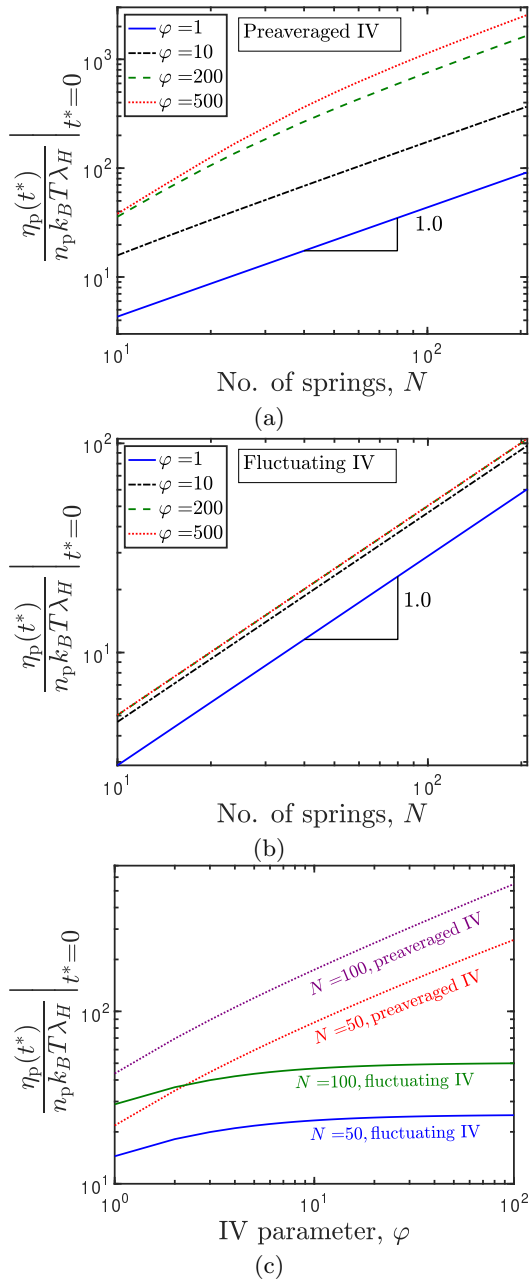


FIG. 4. Stress jump as a function of chain length for (a) preaveraged IV and (b) fluctuating IV models. In (c) the stress jump is plotted as a function of the internal friction parameter, for two different chain lengths. Preaveraged model results are given by Eq. (26), while the fluctuating IV predictions are obtained using the semi-analytical approximation given by Manke and Williams²⁰.

a given chain length, independent of the internal friction parameter. Our recent work³³ shows that Rouse chains with fluctuating IV, however, exhibit a shear-thinning followed by a shear-thickening of the steady-state viscosity with respect to the shear rate, with the internal friction parameter governing the onset and extent of the

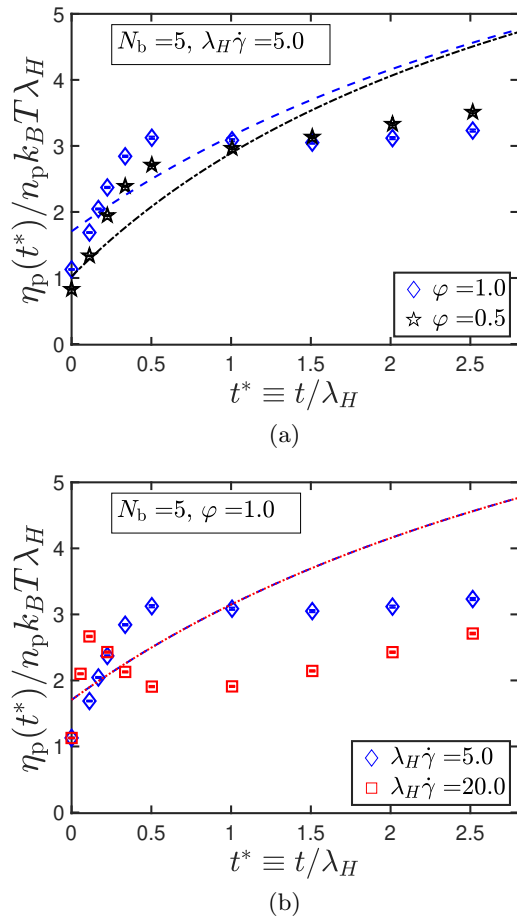


FIG. 5. The effect of (a) internal friction parameter, and (b) shear rate on the time evolution of the dimensionless shear viscosity for a five-bead Rouse chain internal friction. Lines correspond to preaveraged model predictions given by Eq. (24). Symbols are BD simulation results on the Rouse model with fluctuating internal friction.

observed shear-thickening.

It is therefore clear that fluctuations significantly affect the dynamics of polymer molecules away from equilibrium. While a majority of experiments and simulations^{14,17,28–30} over the last two decades on understanding the effects of internal friction on biomolecule dynamics have focused on equilibrium measurements, such as reconfiguration and folding times, the effect of this phenomenon on the probability distribution of polymer extensions in coil-stretch transitions during turbulent flow has recently garnered attention⁴⁷. We anticipate that the present work will provide a theoretical framework for discerning the effects of internal friction in out-of-equilibrium systems. Quantitative comparisons against experiments would require the incorporation of hydrodynamic interaction effects^{48,49}. However, the solution of coarse-grained models which account for fluctuations in both internal viscosity and hydrodynamic interac-

tions (with more than two beads⁵), have additional challenges³³ that have not been addressed so far.

- ¹Kuhn, W. & Kuhn, H. Bedeutung beschränkt freier Drehbarkeit für die Viskosität und Strömungsdoppelbrechung von Fadenmoleküllösungen I. *Helv. Chim. Acta* **28**, 1533–1579 (1945).
- ²Booij, H. C. & van Wiechen, P. H. Effect of Internal Viscosity on the Deformation of a Linear Macromolecule in a Sheared Solution. *J. Chem. Phys.* **52**, 5056–5068 (1970).
- ³de Gennes, P.-G. *Scaling Concepts in Polymer Physics* (Cornell University Press, 1979).
- ⁴Ansari, A., Jones, C. M., Henry, E. R., Hofrichter, J. & Eaton, W. A. The Role of Solvent Viscosity in the Dynamics of Protein Conformational Changes. *Science* **256**, 1796–1798 (1992).
- ⁵Kailasham, R., Chakrabarti, R. & Prakash, J. R. Rheological consequences of wet and dry friction in a dumbbell model with hydrodynamic interactions and internal viscosity. *J. Chem. Phys.* **149**, 094903 (2018).
- ⁶Kailasham, R., Chakrabarti, R. & Prakash, J. R. Wet and dry internal friction can be measured with the Jarzynski equality. *Phys. Rev. Res.* **2**, 013331 (2020).
- ⁷Bird, R. B., Curtiss, C. F., Armstrong, R. C. & Hassager, O. *Dynamics of Polymeric Liquids - Volume 2 : Kinetic Theory* (John Wiley and Sons, New York, 1987).
- ⁸Prakash, J. R. The kinetic theory of dilute solutions of flexible polymers: Hydrodynamic interaction. In Siginer, D. A., De Kee, D. & Chhabra, R. P. (eds.) *Rheology Series*, vol. 8, 467–517 (Elsevier, 1999).
- ⁹Cellmer, T., Henry, E. R., Hofrichter, J. & Eaton, W. A. Measuring internal friction of an ultrafast-folding protein. *Proc. Natl. Acad. Sci. U.S.A.* **105**, 18320–18325 (2008).
- ¹⁰de Sancho, D., Sirur, A. & Best, R. B. Molecular origins of internal friction effects on protein-folding rates. *Nat. Commun.* **5**, 4307 (2014).
- ¹¹Samanta, N., Ghosh, J. & Chakrabarti, R. Looping and reconfiguration dynamics of a flexible chain with internal friction. *AIP Adv.* **4**, 067102 (2014).
- ¹²Samanta, N. & Chakrabarti, R. Reconfiguration dynamics in folded and intrinsically disordered protein with internal friction: Effect of solvent quality and denaturant. *Physica A* **450**, 165–179 (2016).
- ¹³Qiu, L. & Hagen, S. J. A Limiting Speed for Protein Folding at Low Solvent Viscosity. *J. Am. Chem. Soc.* **126**, 3398–3399 (2004).
- ¹⁴Wensley, B. G. *et al.* Experimental evidence for a frustrated energy landscape in a three-helix-bundle protein family. *Nature* **463**, 685–688 (2010).
- ¹⁵Hagen, S. J. Solvent viscosity and friction in protein folding dynamics. *Curr. Protein Pept. Sci.* **11**, 385–395 (2010).
- ¹⁶Borgia, A. *et al.* Localizing internal friction along the reaction coordinate of protein folding by combining ensemble and single-molecule fluorescence spectroscopy. *Nat. Commun.* **3**, 1195–1199 (2012).
- ¹⁷Soranno, A. *et al.* Quantifying internal friction in unfolded and intrinsically disordered proteins with single-molecule spectroscopy. *Proc. Natl. Acad. Sci. U.S.A.* **109**, 17800–17806 (2012).
- ¹⁸Soranno, A. *et al.* Integrated view of internal friction in unfolded proteins from single-molecule FRET, contact quenching, theory, and simulations. *Proc. Natl. Acad. Sci. U.S.A.* **114**, E1833–E1839 (2017).
- ¹⁹Socol, M. *et al.* Rouse model with transient intramolecular contacts on a timescale of seconds recapitulates folding and fluctuation of yeast chromosomes. *Nucleic Acids Res* **47**, 6195–6207 (2019).
- ²⁰Manke, C. W. & Williams, M. C. Stress Jump at the Inception of Shear and Elongational Flows of Dilute Polymer Solutions, Due to Internal Viscosity. *J. Rheol.* **31**, 495–510 (1988).
- ²¹Dasbach, T. P., Manke, C. W. & Williams, M. C. Complex viscosity for the rigorous formulation of the multibead internal

- viscosity model with hydrodynamic interaction. *J. Phys. Chem.* **96**, 4118–4125 (1992).
- ²²Gerhardt, L. J. & Manke, C. W. Relationships among shear stress jumps and high-frequency dynamic viscosity of viscoelastic fluids. *J. Rheol.* **38**, 1227–1234 (1994).
- ²³Alexander-Katz, A., Wada, H. & Netz, R. R. Internal friction and nonequilibrium unfolding of polymeric globules. *Phys. Rev. Lett.* **103**, 028102 (2009).
- ²⁴Schulz, J. C. F., Miettinen, M. S. & Netz, R. R. Unfolding and Folding Internal Friction of β -Hairpins Is Smaller than That of α -Helices. *J. Phys. Chem. B* **119**, 4565–4574 (2015).
- ²⁵Murayama, Y., Wada, H. & Sano, M. Dynamic force spectroscopy of a single condensed DNA. *Eur. Phys. Lett.* **79**, 58001 (2007).
- ²⁶Khatri, B. S., Kawakami, M., Byrne, K., Smith, D. A. & McLeish, T. C. B. Entropy and barrier-controlled fluctuations determine conformational viscoelasticity of single biomolecules. *Biophys. J.* **92**, 1825–1835 (2007).
- ²⁷Guérin, T., Bénichou, O. & Voituriez, R. Non-Markovian polymer reaction kinetics. *Nat. Chem.* **4**, 568–573 (2012).
- ²⁸Cheng, R. R., Hawk, A. T. & Makarov, D. E. Exploring the role of internal friction in the dynamics of unfolded proteins using simple polymer models. *J. Chem. Phys.* **138**, 074112 (2013).
- ²⁹Schulz, J. C. F., Schmidt, L., Best, R. B., Dzubiella, J. & Netz, R. R. Peptide Chain Dynamics in Light and Heavy Water: Zooming in on Internal Friction. *J. Am. Chem. Soc.* **134**, 6273–6279 (2012).
- ³⁰Ameseder, F. *et al.* Relevance of Internal Friction and Structural Constraints for the Dynamics of Denatured Bovine Serum Albumin. *J. Phys. Chem. Lett.* **9**, 2469–2473 (2018).
- ³¹Soranno, A., Zosel, F. & Hofmann, H. Internal friction in an intrinsically disordered protein—Comparing Rouse-like models with experiments. *J. Chem. Phys.* **148**, 123326 (2018).
- ³²Khatri, B. S. & McLeish, T. C. B. Rouse model with internal friction: A coarse grained framework for single biopolymer dynamics. *Macromolecules* **40**, 6770–6777 (2007).
- ³³Kailasham, R., Chakrabarti, R. & Prakash, J. R. Rouse model with fluctuating internal friction (2021). Preprint at <https://arxiv.org/abs/2102.09112>.
- ³⁴Poirier, M. G. & Marko, J. F. Effect of Internal Friction on Biofilament Dynamics. *Phys. Rev. Lett.* **88**, 228103 (2002).
- ³⁵Mondal, D., Adhikari, R. & Sharma, P. Internal friction controls active ciliary oscillations near the instability threshold. *Sci. Adv.* **6**, eabb0503 (2020).
- ³⁶Nandagiri, A. *et al.* Flagellar energetics from high-resolution imaging of beating patterns in tethered mouse sperm (2020). Preprint at <https://doi.org/10.1101/2020.08.31.269340>.
- ³⁷Bekard, I. B., Asimakis, P., Bertolini, J. & Dunstan, D. E. The effects of shear flow on protein structure and function. *Biopolymers* **95**, 733–745 (2011).
- ³⁸Öttinger, H. C. *Stochastic Processes in Polymeric Fluids* (Springer, Berlin, 1996).
- ³⁹Doi, M. & Edwards, S. F. *The Theory of Polymer Dynamics* (Clarendon, Oxford, 1986).
- ⁴⁰Fixman, M. Dynamics of stiff polymer chains. *J. Chem. Phys.* **89**, 2442 (1988).
- ⁴¹Des Cloizeaux, J. Short range correlation between elements of a long polymer in a good solvent. *J. Phys. France* **10**, 223–238 (1980).
- ⁴²Toan, N. M., Morrison, G., Hyeon, C. & Thirumalai, D. Kinetics of loop formation in polymer chains. *J. Phys. Chem. B* **112**, 6094–6106 (2008).
- ⁴³Kumari, K., Prakash, J. R. & Padinhateeri, R. Spatiotemporal organization of chromatin domains: role of interaction energy and polymer entropy (2021). Preprint at <https://arxiv.org/abs/2102.09123>.
- ⁴⁴Qiu, L., Pabit, S. A., Roitberg, A. E. & Hagen, S. J. Smaller and faster: The 20-residue Trp-cage protein folds in 4 μ s. *J. Am. Chem. Soc.* **124**, 12952–12953 (2002).
- ⁴⁵Schieber, J. D. & Öttinger, H. C. On consistency criteria for stress theory models tensors in kinetic. *J. Rheol.* **38**, 1909 (1994).
- ⁴⁶Hua, C. C. & Schieber, J. D. Nonequilibrium Brownian dynamics simulations of Hookean and FENE dumbbells with internal viscosity. *J. Non-Newtonian Fluid Mech.* **56**, 307–332 (1995).
- ⁴⁷Vincenzi, D. Effect of internal friction on the coil–stretch transition in turbulent flows. *Soft Matter* – (2021).
- ⁴⁸Sasmal, C., Hsiao, K.-W., Schroeder, C. M. & Prakash, J. R. Parameter-free prediction of DNA dynamics in planar extensional flow of semidilute solutions. *J. Rheol.* **61**, 169 (2017).
- ⁴⁹Prakash, J. R. Universal dynamics of dilute and semidilute solutions of flexible linear polymers. *Curr. Opin. Colloid Interface Sci.* **43**, 63–79 (2019).
- ⁵⁰Verdier, P. H. Monte carlo studies of lattice-model polymer chains. i. correlation functions in the statistical-bead model. *J. Chem. Phys.* **45**, 2118–2121 (1966).
- ⁵¹Kopf, A., Dünweg, B. & Paul, W. Dynamics of polymer “isotope” mixtures: Molecular dynamics simulation and Rouse model analysis. *J. Chem. Phys.* **107**, 6945–6955 (1997).

METHODS

$$\sum_n \Omega_{\mu n} \Omega_{\nu n} = \delta_{\mu\nu} \quad (10)$$

Analytical solutions

The Rouse matrix in Eq. (2) is of size $N_b \times N_b$ and has the following structure

$$\mathbf{A}^{(R)} = \begin{pmatrix} 1 & -1 & 0 & \cdots & 0 \\ -1 & 2 & -1 & 0 & \cdots & 0 \\ 0 & -1 & 2 & -1 & \cdots & \\ \vdots & \vdots & \vdots & & & \\ 0 & 0 & \cdots & -1 & 2 & -1 \\ 0 & 0 & \cdots & 0 & -1 & 1 \end{pmatrix} \quad (7)$$

The elements of the orthogonal matrix $\mathbf{\Omega}$ which project the bead-positions into normal-mode space are given by^{50,51}

$$\Omega_{\mu n} = \left(\frac{2 - \delta_{n0}}{N_b} \right)^{1/2} \cos \left[\left(\mu - \frac{1}{2} \right) \frac{n\pi}{N_b} \right] \quad (8)$$

where $\mu = 1, 2, 3, \dots, N_b$ and $n = 0, 1, 2, \dots, (N_b - 1)$. The columns of $\mathbf{\Omega}$ are eigenvectors of $\mathbf{A}^{(R)}$, which means

$$\sum_{\mu} \Omega_{\mu m} \Omega_{\mu n} = \delta_{mn} \quad (9)$$

Using the inverse transformation $\mathbf{r}_{\mu}(t) = \sum_{j=0}^{N_b-1} \Omega_{\mu j} \mathbf{X}_j(t)$, the definition $\mathbf{R}_{\mu\nu}(t) \equiv \mathbf{r}_{\nu}(t) - \mathbf{r}_{\mu}(t)$, and

$$\langle \mathbf{X}_p(0) \cdot \mathbf{X}_q(t) \rangle = \frac{3k_B T}{H_p} \delta_{pq} e^{-t/\tau_p}, \quad (15)$$

the normalized autocorrelation at equilibrium ($\boldsymbol{\kappa} = \mathbf{0}$) may be derived to be

$$\frac{\langle \mathbf{R}_{\mu\nu}(0) \cdot \mathbf{R}_{\mu\nu}(t) \rangle}{\langle \mathbf{R}_{\mu\nu}^2(0) \rangle} = \left[\frac{2}{N_b(N_b - 1)} \right] \left[\sum_{p=1}^{N_b-1} \left\{ \cos \left[\left(\nu - \frac{1}{2} \right) \frac{p\pi}{N_b} \right] - \cos \left[\left(\mu - \frac{1}{2} \right) \frac{p\pi}{N_b} \right] \right\}^2 \left(\frac{1}{a_p} \right) e^{-t/\tau_p} \right] \quad (16)$$

which may be non-dimensionalized, using the length and time-scales given by $l_H = \sqrt{k_B T / H}$ and $\lambda_H = \zeta / 4H$, respectively, to yield

$$\frac{\langle \mathbf{R}_{\mu\nu}^*(0) \cdot \mathbf{R}_{\mu\nu}^*(t^*) \rangle}{\langle \mathbf{R}_{\mu\nu}^{*2}(0) \rangle} = \left[\frac{2}{N_b |\nu - \mu|} \right] \sum_{p=1}^{N_b-1} \left\{ \cos \left[\left(\nu - \frac{1}{2} \right) \frac{p\pi}{N_b} \right] - \cos \left[\left(\mu - \frac{1}{2} \right) \frac{p\pi}{N_b} \right] \right\}^2 \left(\frac{1}{a_p} \right) \exp \left[- \left(\frac{a_p}{1 + \theta a_p} \right) \frac{t^*}{4} \right] \quad (17)$$

For the special case of the end-to-end vector, $\mathbf{R}_E(t) \equiv \mathbf{R}_{1N_b}(t)$, we have

$$\frac{\langle \mathbf{R}_E^*(0) \cdot \mathbf{R}_E^*(t^*) \rangle}{\langle \mathbf{R}_E^{*2}(0) \rangle} = \left[\frac{8}{N_b(N_b - 1)} \right] \sum_{p:\text{odd}}^{N_b-1} \cos^2 \left(\frac{p\pi}{2N_b} \right) \left(\frac{1}{a_p} \right) \exp \left[- \left(\frac{a_p}{1 + \theta a_p} \right) \frac{t^*}{4} \right] \quad (18)$$

The detailed steps for the derivation of Eqs. (17) and (18), starting from Eq. (13), have been presented in Sec. II A of the Supplementary Material. As detailed in Sec. II B of the Supplementary Material, an expression for the time evolution of the mean-squared end-to-end distance for the continuum RIF model in simple shear flow may be derived

where a_m refers to the eigenvalues of $\mathbf{A}^{(R)}$, given by

$$a_m = 4 \sin^2 \left(\frac{m\pi}{2N_b} \right); \quad m = 0, 1, 2, \dots, (N_b - 1) \quad (12)$$

Applying the transformation to normal co-ordinates, $\mathbf{X}_j(t) = \sum_{\mu} \Omega_{\mu j} \mathbf{r}_{\mu}(t)$, to Eq. (2), the governing equation in normal-mode coordinates becomes

$$\frac{d\mathbf{X}_p}{dt} = - \frac{H a_p}{\zeta (1 + \theta a_p)} \mathbf{X}_p + \left(\frac{1}{1 + \theta a_p} \right) \boldsymbol{\kappa} \cdot \mathbf{X}_p + \mathbf{g}_p(t) \quad (13)$$

where $\theta = (K/3\zeta) = \varphi/3$, and the moments of the noise vector, $\mathbf{g}_p(t)$, are given as follows

$$\langle g_p^\alpha \rangle = 0; \quad \langle g_p^\alpha(t) g_q^\beta(t') \rangle = \frac{2k_B T}{\zeta_p} \delta_{pq} \delta^{\alpha\beta} \delta(t - t') \quad (14)$$

with $H_p = H a_p$, $\zeta_p = \zeta (1 + \theta a_p)$ and $\tau_p = \zeta_p / H_p$. The indices α and β in Eq. (14) run from 1 to d , where d denotes the dimensionality of the system. The present work considers only the $d = 3$ case.

to be

$$\frac{\langle \mathbf{R}_E^{*2}(t^*) \rangle}{\langle \mathbf{R}_E^{*2} \rangle_{\text{eq}}} = \left[\frac{8}{N_b(N_b - 1)} \right] \sum_{p:\text{odd}}^{N_b-1} \left(\frac{1}{a_p} \right) \cos^2 \left(\frac{p\pi}{2N_b} \right) \times \left\{ 1 + \frac{8(\lambda_H \dot{\gamma})^2}{3a_p^2} \left[1 - \left(\exp \left[- \left(\frac{a_p}{1 + \theta a_p} \right) \frac{t^*}{2} \right] \left[1 + \left(\frac{a_p}{1 + \theta a_p} \right) \frac{t^*}{2} \right] \right) \right] \right\} \quad (19)$$

where $\langle \mathbf{R}_E^{*2} \rangle_{\text{eq}} = 3(N_b - 1)$ is the mean-squared value for the end-to-end vector at equilibrium. The steady state value is obtained by taking the limit $t^* \rightarrow \infty$ in Eq. (19) to give

$$\frac{\langle \mathbf{R}_E^{*2} \rangle}{\langle \mathbf{R}_E^{*2} \rangle_{\text{eq}}} = \left[\frac{8}{N_b(N_b - 1)} \right] \sum_{p:\text{odd}}^{N_b-1} \left(\frac{1}{a_p} \right) \cos^2 \left(\frac{p\pi}{2N_b} \right) \left\{ 1 + \frac{8(\lambda_H \dot{\gamma})^2}{3a_p^2} \right\} \quad (20)$$

The root-mean-squared difference between the exact BD simulation results (with fluctuating IV) for the normalized autocorrelation of $\mathbf{R}_{\mu\nu}^*$ and the preaveraged result given by Eq. (17) may be quantified as

$$\Delta = \sqrt{\frac{1}{N_{\text{points}}} \sum_{i=1}^{N_{\text{points}}} \left[y_i^{(\text{BD})} - y_i^{(\text{analytical})} \right]^2} \quad (21)$$

where $y_i^{(\text{BD}/\text{analytical})}$ refers to the simulation/analytical result at the i^{th} datapoint, with N_{points} the number of time-instances at which the simulation results have been obtained.

Preaveraged internal viscosity model

The detailed steps for the derivation of the governing stochastic differential equation for the Rouse model with preaveraged internal friction has been presented in Sec. III A of the Supplementary Material. It takes the form

$$d\mathbf{Q}_k^* = \left(\frac{1}{1 + 2\theta} \right) \left[\sum_{l=1}^N \Lambda_{kl} (\boldsymbol{\kappa}^* \cdot \mathbf{Q}_l^*) - \left(\frac{1}{4} \right) \sum_{l=1}^N J_{kl} \mathbf{Q}_l^* \right] dt^* + \sqrt{\frac{1}{2(1 + 2\theta)}} \sum_{l=1}^N B_{kl} d\mathbf{W}_l^*, \quad (22)$$

where $N = N_b - 1$ represents the number of springs in the chain, $1 \leq k \leq N$, $\sum_{j=1}^N B_{kj} B_{lj} = J_{kl}$, and $d\mathbf{W}_l^*$ is a three-dimensional Wiener process. The quantities Λ_{kl} and J_{kl} are functions only of the internal friction parameter θ , and depend neither on the chain reconfiguration, nor on the flow strength. In the absence of internal friction, $\Lambda_{kl} = \delta_{kl}$, and $J_{kl} = A_{kl}$, where

$$A_{kl} = \begin{cases} 2; & k = l \\ -1; & |k - l| = 1 \\ 0; & \text{otherwise} \end{cases} \quad (23)$$

The notations \mathbf{A} and \mathbf{J} are introduced to indicate $N \times N$ matrices whose elements are given by Λ_{kl} and J_{kl} , respectively. The precise definitions of Λ_{kl} and J_{kl} have

been given in the Supplementary Material. The preaveraged IV model may also be solved semi-analytically, as described in Sec. III B of the Supplemental Material, by numerically evaluating the orthogonal matrix that would project the connector vectors into normal mode space.

As detailed in Sec III C of the Supplementary Material, the time-evolution of the shear-viscosity for the preaveraged model may be evaluated to be

$$\frac{\eta_p(t^*)}{n_p k_B T \lambda_H} = \left(\frac{1}{1 + 2\theta} \right) \sum_{m,n,q=1}^N \Pi_{mq} \mathcal{L}_{mn} \Pi_{nq} I_q(t^*) + 2 \text{tr} \left[\mathbf{C} - \frac{1}{1 + 2\theta} \mathbf{S} \right]; \quad (24)$$

with

$$I_q(t^*) = 2 \left(\frac{\tilde{b}_q}{\tilde{a}_q} \right) \left\{ 1 - \exp \left[- \left(\frac{\tilde{a}_q}{1 + 2\theta} \right) \frac{t^*}{2} \right] \right\} \quad (25)$$

where \mathbf{C} denotes the Kramers matrix⁷, $\mathcal{L} = \mathbf{J} \cdot \mathbf{C}$, $\mathbf{S} = \mathbf{A} \cdot \mathbf{C}$, and \tilde{a}_q and \tilde{b}_q represent the eigenvalues of \mathbf{J} and \mathbf{A} , respectively. The matrix $\mathbf{\Pi}$ diagonalizes \mathbf{J} , as $\sum_{l,n=1}^N \Pi_{lj} J_{ln} \Pi_{nk} = \tilde{a}_j \delta_{jk}$. The validity of Eq. (24) has been established by comparison against BD simulations on the model with preaveraged IV, as shown in Fig. S5 of the Supplementary Material. From Eq. 25, it is clear that the function $I_q(t^*) \rightarrow 0$ as $t^* \rightarrow 0$, and Eq. (24) reduces to

$$\frac{\eta_p(t^*)}{n_p k_B T \lambda_H} \Big|_{t^*=0} = 2 \text{tr} \left[\mathbf{C} - \frac{1}{1 + 2\theta} \mathbf{S} \right] \quad (26)$$

ACKNOWLEDGEMENTS

Numerical simulations were performed on the MonARCH and MASSIVE computer clusters of Monash University, and the SpaceTime-2 computational facility of IIT Bombay. R. C. acknowledges SERB for funding (Project No. MTR/2020/000230 under MATRICS scheme). We also acknowledge the funding and general support received from the IITB-Monash Research Academy.

AUTHOR CONTRIBUTIONS

R.K., R.C., and J.R.P. designed research, performed research, contributed new reagents/analytic tools, analyzed data, and wrote the paper.

COMPETING INTERESTS

The authors declare no competing interests.

Supplementary Material for: How important are fluctuations in the treatment of internal friction in polymers?

R. Kailasham,^{1,2,3} Rajarshi Chakrabarti*,^{2, a)} and J. Ravi Prakash*^{3, b)}

¹⁾*IITB-Monash Research Academy, Indian Institute of Technology Bombay, Mumbai, Maharashtra - 400076, India*

²⁾*Department of Chemistry, Indian Institute of Technology Bombay, Mumbai, Maharashtra - 400076, India*

³⁾*Department of Chemical Engineering, Monash University, Melbourne, VIC 3800, Australia*

I. INTRODUCTION

The main paper examines the importance of fluctuations in the treatment of internal friction, by comparing preaveraged model predictions with the predictions of a model with fluctuations, for observables both at equilibrium and in simple shear flow. The details corresponding to various aspects of the investigation are presented here.

This document is organized as follows. Section II presents the discrete version of the Rouse model with internal friction (RIF), which is a finite-bead representation of the model introduced by McLeish and coworkers¹, and accounts for the presence of a flow term. Using normal mode analysis, the autocorrelation of the end to end vector at equilibrium, and the time evolution of the mean-squared end-to-end distance in shear flow have been derived in Secs. II A and II B, respectively. In Sec. III, the principles of polymer kinetic theory^{2,3} are used to derive the governing stochastic differential equation for a Rouse chain with preaveraged internal friction [Sec. III A], by applying the decoupling methodology outlined in our recent work [Ref. 4, under review]. Observables at equilibrium [Sec. III B] and in flow [Sec. III C] have been derived using normal mode analysis.

II. DISCRETE VERSION OF ROUSE MODEL WITH INTERNAL FRICTION

The Langevin equation for the μ^{th} bead of a discrete Rouse chain with internal friction¹ is given by

$$\frac{d\mathbf{r}_\mu}{dt} = -\left(\frac{H}{\zeta} + \frac{K}{3\zeta} \frac{d}{dt}\right) \sum_{\nu=1}^{N_b} A_{\mu\nu}^{(\text{R})} \mathbf{r}_\nu + \boldsymbol{\kappa} \cdot \mathbf{r}_\mu + \boldsymbol{\xi}_\mu \quad (1)$$

where H is the Hookean spring constant, $(K/3)$ is the dashpot coefficient, ζ is the monomeric friction coefficient, $\boldsymbol{\kappa}$ indicates the flow-field, $\boldsymbol{\xi}_\mu$ represents the noise term, and $A_{\mu\nu}^{(\text{R})}$ are elements of the connectivity matrix

of size $N_b \times N_b$, which has the form⁵

$$\mathbf{A}^{(\text{R})} = \begin{pmatrix} 1 & -1 & 0 & \cdots & 0 \\ -1 & 2 & -1 & 0 & \cdots & 0 \\ 0 & -1 & 2 & -1 & \cdots & \\ \vdots & \vdots & \vdots & & & \\ 0 & 0 & \cdots & -1 & 2 & -1 \\ 0 & 0 & \cdots & 0 & -1 & 1 \end{pmatrix} \quad (2)$$

The elements of the orthogonal matrix $\boldsymbol{\Omega}$ which project the bead-positions into normal-mode space are given by^{5,6}

$$\Omega_{\mu n} = \left(\frac{2 - \delta_{n0}}{N_b}\right)^{1/2} \cos\left[\left(\mu - \frac{1}{2}\right) \frac{n\pi}{N_b}\right] \quad (3)$$

where $\mu = 1, 2, 3, \dots, N_b$ and $n = 0, 1, 2, \dots, (N_b - 1)$. The columns of $\boldsymbol{\Omega}$ are eigenvectors of $\mathbf{A}^{(\text{R})}$, which means

$$\begin{aligned} \sum_{\mu} \Omega_{\mu m} \Omega_{\mu n} &= \delta_{mn} \\ \sum_n \Omega_{\mu n} \Omega_{\nu n} &= \delta_{\mu\nu} \\ \sum_{\mu} \sum_{\nu} \Omega_{\mu n} A_{\mu\nu} \Omega_{\nu m} &= a_m \delta_{nm} \end{aligned} \quad (4)$$

where a_m refers to the eigenvalues of $\mathbf{A}^{(\text{R})}$, given by

$$a_m = 4 \sin^2\left(\frac{m\pi}{2N_b}\right); \quad m = 0, 1, 2, \dots, (N_b - 1) \quad (5)$$

The length- and time-scales for this coarse-grained model are defined to be $l_H = \sqrt{k_B T / H}$, and $\lambda_H = \zeta / 4H$, respectively, where k_B is Boltzmann's constant and T the absolute temperature. Quantities non-dimensionalized using these scales are denoted with an asterisk as superscript. The internal friction coefficient is given by $\varphi = K/\zeta$, and we additionally define $\theta = (K/3\zeta) = \varphi/3$.

A. At equilibrium

In this section, we present the derivation for the autocorrelation of the end-to-end vector at equilibrium, by first setting $\boldsymbol{\kappa} = 0$ in Eq. (1). The transformation to normal co-ordinates, \mathbf{X}_j is given by^{5,6} $\mathbf{X}_j = \sum_{\mu} \Omega_{\mu j} \mathbf{r}_\mu$,

^{a)}Electronic mail: rajarshi@chem.iitb.ac.in

^{b)}Electronic mail: ravi.jagadeeshan@monash.edu

and the governing equation in normal-mode coordinates becomes

$$\frac{d\mathbf{X}_p}{dt} = -\frac{H_p}{\zeta_p}\mathbf{X}_p + \mathbf{g}_p(t) \quad (6)$$

where the moments of the noise vector, $\mathbf{g}_p(t)$, are given as follows

$$\langle g_p^\alpha \rangle = 0; \quad \langle g_p^\alpha(t)g_q^\beta(t') \rangle = \frac{2k_B T}{\zeta_p} \delta_{pq} \delta^{\alpha\beta} \delta(t-t') \quad (7)$$

with $H_p = Ha_p$, and $\zeta_p = \zeta(1 + \theta a_p)$. The indices α and β in Eq. (7) run from 1 to d , where d denotes

the dimensionality of the system. For the rest of this paper, we shall concern ourselves with the $d = 3$ case. Eq. (6) represents the equation of motion of a Brownian harmonic oscillator moving in a potential of stiffness H_p and experiencing a friction coefficient ζ_p . For such an oscillator, it is known that⁵⁻⁷

$$\langle \mathbf{X}_p(0) \cdot \mathbf{X}_q(t) \rangle = \frac{3k_B T}{H_p} \delta_{pq} e^{-t/\tau_p} \quad (8)$$

where

$$\tau_p = \zeta_p/H_p = (\zeta/4H) \sin^{-2}(p\pi/2N_b) + (K/3H) \quad (9)$$

The expressions for the bead position vectors in terms of the normal coordinates is given as

$$\mathbf{r}_\mu = \sum_{j=0}^{N_b-1} \Omega_{\mu j} \mathbf{X}_j(t) \quad (10)$$

and the vector joining beads μ and ν is written as

$$\mathbf{R}_{\mu\nu}(t) \equiv \mathbf{r}_\nu(t) - \mathbf{r}_\mu(t) = \sqrt{\frac{2}{N_b}} \sum_{q=1}^{N_b-1} \left\{ \cos \left[\left(\nu - \frac{1}{2} \right) \frac{q\pi}{N_b} \right] - \cos \left[\left(\mu - \frac{1}{2} \right) \frac{q\pi}{N_b} \right] \right\} \mathbf{X}_q(t) \quad (11)$$

from which the expression for its autocorrelation may be written as

$$\begin{aligned} \langle \mathbf{R}_{\mu\nu}(0) \cdot \mathbf{R}_{\mu\nu}(t) \rangle &= \left(\frac{2}{N_b} \right) \sum_{q=1}^{N_b-1} \sum_{p=1}^{N_b-1} \left\{ \cos \left[\left(\nu - \frac{1}{2} \right) \frac{q\pi}{N_b} \right] - \cos \left[\left(\mu - \frac{1}{2} \right) \frac{q\pi}{N_b} \right] \right\} \\ &\quad \times \left\{ \cos \left[\left(\nu - \frac{1}{2} \right) \frac{p\pi}{N_b} \right] - \cos \left[\left(\mu - \frac{1}{2} \right) \frac{p\pi}{N_b} \right] \right\} \langle \mathbf{X}_p(0) \cdot \mathbf{X}_q(t) \rangle \end{aligned} \quad (12)$$

The choice of the noise term in normal mode space [Eq. (7)] ensures that the mean-squared value of the segmental vector $\mathbf{R}_{\mu\nu}$ at equilibrium is given by $\langle \mathbf{R}_{\mu\nu}^2 \rangle_{\text{eq}} \equiv \langle \mathbf{R}_{\mu\nu}^2(0) \rangle = 3|\nu - \mu|(k_B T/H)$. Using Eqs. (8) and (12), the normalized autocorrelation for the discrete RIF model may be written as follows

$$\frac{\langle \mathbf{R}_{\mu\nu}(0) \cdot \mathbf{R}_{\mu\nu}(t) \rangle}{\langle \mathbf{R}_{\mu\nu}^2(0) \rangle} = \left[\frac{2}{N_b(N_b-1)} \right] \left[\sum_{p=1}^{N_b-1} \left\{ \cos \left[\left(\nu - \frac{1}{2} \right) \frac{p\pi}{N_b} \right] - \cos \left[\left(\mu - \frac{1}{2} \right) \frac{p\pi}{N_b} \right] \right\}^2 \left(\frac{1}{a_p} \right) e^{-t/\tau_p} \right] \quad (13)$$

For the special case of the end-to-end vector, $\mathbf{R}_E(t) \equiv \mathbf{R}_{1N_b}(t)$, the normalized autocorrelation is given by

$$\frac{\langle \mathbf{R}_E(0) \cdot \mathbf{R}_E(t) \rangle}{\langle \mathbf{R}_E^2(0) \rangle} = \left[\frac{8}{N_b(N_b-1)} \right] \left[\sum_{p:\text{odd}}^{N_b-1} \cos^2 \left(\frac{p\pi}{2N_b} \right) \left(\frac{1}{a_p} \right) e^{-t/\tau_p} \right] \quad (14)$$

Using Eq. (9), we may write

$$\frac{t}{\tau_p} \equiv \frac{H_p t}{\zeta_p} = \left(\frac{Ha_p t}{\zeta(1 + \theta a_p)} \right) = \left(\frac{Ha_p t}{4H\lambda_H(1 + \theta a_p)} \right) = \left(\frac{1}{4} \right) \left(\frac{a_p}{1 + \theta a_p} \right) \left(\frac{t}{\lambda_H} \right) = \left(\frac{a_p}{1 + \theta a_p} \right) \frac{t^*}{4} \quad (15)$$

and

$$\frac{t}{\tau_p} \equiv \left(\frac{1 + \theta a_1}{1 + \theta a_p} \right) \left(\frac{a_p}{a_1} \right) \left(\frac{t}{\tau_1} \right), \quad (16)$$

The dimensionless, normalized autocorrelation of the end-to-end vector may therefore be rewritten as

$$\frac{\langle \mathbf{R}_E^*(0) \cdot \mathbf{R}_E^*(t^*) \rangle}{\langle \mathbf{R}_E^{*2}(0) \rangle} = \left[\frac{8}{N_b(N_b - 1)} \right] \sum_{p:\text{odd}}^{N_b-1} \cos^2 \left(\frac{p\pi}{2N_b} \right) \left(\frac{1}{a_p} \right) \exp \left[- \left(\frac{a_p}{1 + \theta a_p} \right) \frac{t^*}{4} \right] \quad (17)$$

In terms of t/τ_1 , the autocorrelation is given to be

$$\frac{\langle \mathbf{R}_E^*(0) \cdot \mathbf{R}_E^*(t/\tau_1) \rangle}{\langle \mathbf{R}_E^{*2}(0) \rangle} = \left[\frac{8}{N_b(N_b - 1)} \right] \sum_{p:\text{odd}}^{N_b-1} \cos^2 \left(\frac{p\pi}{2N_b} \right) \left(\frac{1}{a_p} \right) \exp \left[- \left(\frac{1 + \theta a_1}{1 + \theta a_p} \right) \left(\frac{a_p}{a_1} \right) \left(\frac{t}{\tau_1} \right) \right] \quad (18)$$

The normalized autocorrelation for the continuum model is as follows^{1,7}

$$\frac{\langle \mathbf{R}_E^*(0) \cdot \mathbf{R}_E^*(t) \rangle}{\langle \mathbf{R}_E^{*2}(0) \rangle} = \left(\frac{8}{\pi^2} \right) \sum_{p:\text{odd}}^{\infty} \left(\frac{1}{p^2} \right) \exp \left[- \frac{t}{\tilde{\tau}_p} \right], \quad (19)$$

where

$$\tilde{\tau}_p = (N_b^2 \zeta / p^2 \pi^2 H) + (K/3H), \quad (20)$$

and the dimensionless mean-squared end-to-end distance at equilibrium is given by $\langle \mathbf{R}_E^{*2}(0) \rangle \equiv \langle \mathbf{R}_E^{*2} \rangle_{\text{eq}} = 3N_b$. The above expression may be rewritten in terms of $t/\tilde{\tau}_1$ as

$$\frac{\langle \mathbf{R}_E^*(0) \cdot \mathbf{R}_E^*(t/\tilde{\tau}_1) \rangle}{\langle \mathbf{R}_E^{*2}(0) \rangle} = \left(\frac{8}{\pi^2} \right) \sum_{p:\text{odd}}^{\infty} \left(\frac{1}{p^2} \right) \exp \left\{ -p^2 \left[\frac{(N_b/\pi)^2 + \theta}{(N_b/\pi)^2 + p^2\theta} \right] \left(\frac{t}{\tilde{\tau}_1} \right) \right\} \quad (21)$$

From Eqs. (9) and (20), and recognizing that $\sin(x) \approx x$ as $x \rightarrow 0$, it is observed that $\tau_p \rightarrow \tilde{\tau}_p$ as $N_b \rightarrow \infty$.

The infinite summation in Eq. (21) runs over all positive odd integers. We define a related quantity $S(N_b, N_t, t/\tilde{\tau}_1)$, as

$$S(N_b, N_t, t/\tilde{\tau}_1) = \sum_{p=1,3,5,\dots}^{2N_t-1} \left(\frac{1}{p^2} \right) \exp \left\{ -p^2 \left[\frac{(N_b/\pi)^2 + \theta}{(N_b/\pi)^2 + p^2\theta} \right] \left(\frac{t}{\tilde{\tau}_1} \right) \right\} \quad (22)$$

In Fig. S1, the variation of S as function of the number of terms included in the summation, N_t , for two different chain lengths, at two values of the dimensionless time and the internal friction parameter are displayed. In Fig. S1 (a), the case without internal friction is presented, and it is clearly seen that the summation requires fewer than ten terms for convergence at both early and later values of time. The summation at later times converges more quickly than the convergence at earlier times, for both two-bead and ten-bead chains. In Fig. S1 (b), the case with internal friction is presented. It is seen that nearly two hundred terms are required for the convergence of the sum for the two-bead chain at early times, and the corresponding number for the ten-bead chain at the same value of scaled time is marginally lower. As seen in (a), the summation at later times require fewer terms for convergence as compared to early times. We henceforth use two hundred terms in the numerical calculation of the infinite sum indicated in Eq. (21).

In Fig. S2, it is seen that the normalized autocorrelation for the discrete model approaches the continuum result as the chain length is increased, for cases with and without internal friction. The difference is

larger at early times, and lesser at later times, for all the values of chain length examined in the figure. In this figure, the normalized autocorrelation for the discrete chain is plotted as a function of time scaled by the longest relaxation time of the discrete chain $[t/\tau_1]$, whereas the autocorrelation for the continuum model is plotted as a function of $t/\tilde{\tau}_1$. The variable s is used to refer to the scaled time, and its exact definition is context-dependent. For the case without internal friction [Fig. S2 (a)], it is clearly seen that the difference between the discrete and continuum result decreases with an increase in the chain length. However, for the case with internal friction [Fig. S2 (b)], the difference appears to be non-monotonic in the chain length.

Fig. S3 examines the variation of the difference between the discrete and continuum result as a function of chain length, at three different instances of the scaled time s , for different values of the internal friction parameter. Note that the difference between the two models is taken at the same value of s . The magnitude of the difference is seen to be larger at shorter times, and smaller at later times, as previously seen in Fig. S2, for models with and without internal friction. However, the nature of the variation of the difference with the

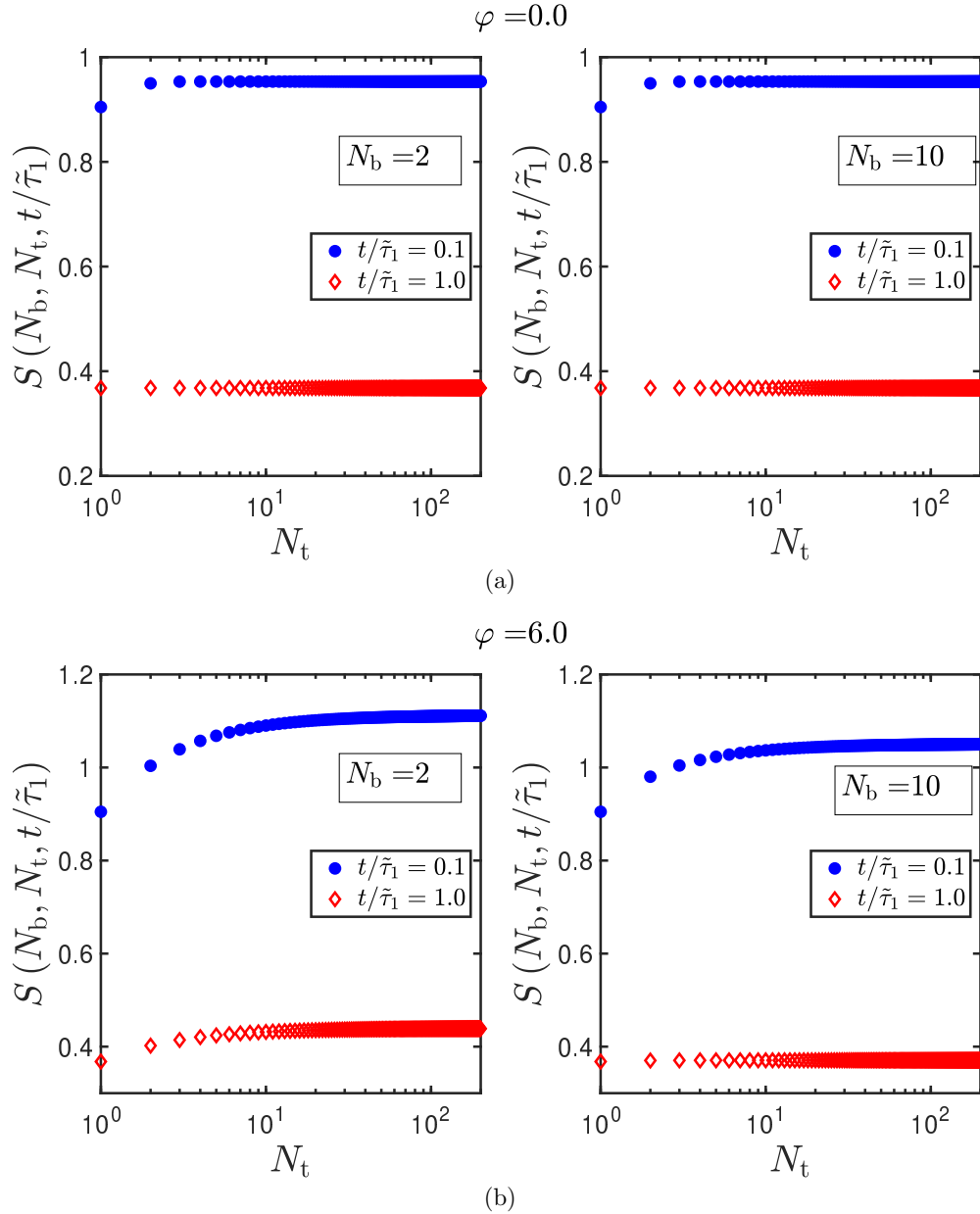


FIG. S1. Plot of number of terms required for convergence of summation indicated by Eq. (22) for two different chain lengths, for models with [(a)] and without [(b)] internal friction, at different values of the scaled time.

chain length is significantly impacted by the presence of internal friction. For cases without internal friction, the difference decreases monotonically with the chain length. With the inclusion of internal friction, however, the difference hits a peak before decreasing monotonically with the chain length. The height of the peak is seen to be diminished at later times.

B. In shear flow

In this section, we present the derivation for the time evolution of mean-squared end-to-end distance of a dis-

crete RIF chain in simple shear flow, by first setting

$$\boldsymbol{\kappa} = \begin{pmatrix} 0 & \dot{\gamma} & 0 \\ 0 & 0 & 0 \\ 0 & 0 & 0 \end{pmatrix} \quad (23)$$

in Eq. (1), where $\dot{\gamma}$ denotes the shear rate. Transforming Eq. (1) into normal-mode coordinates using a procedure identical to that described in Sec. II A, we obtain

$$\frac{d\mathbf{X}_p}{dt} = -\frac{Ha_p}{\zeta(1+\theta a_p)}\mathbf{X}_p + \left(\frac{1}{1+\theta a_p}\right)\boldsymbol{\kappa} \cdot \mathbf{X}_p + \mathbf{g}_p(t) \quad (24)$$

where the moments of the noise vector, $\mathbf{g}_p(t)$, are as defined in Eq. (7). The governing equation may be

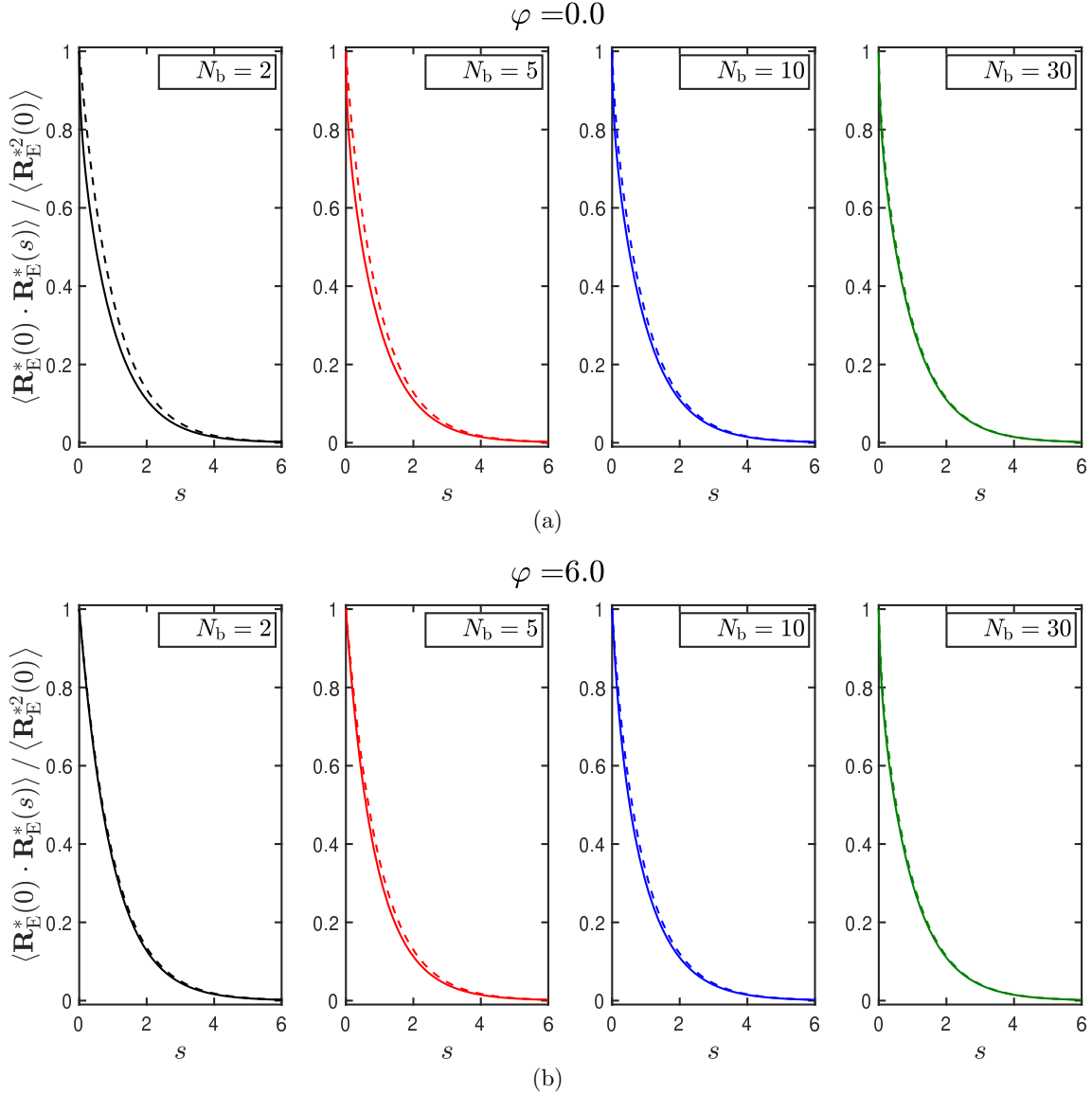


FIG. S2. Comparison of the normalized autocorrelation expressions for the discrete [dashed line, Eq. (18)] and continuum [solid line, Eq. (21)] RIF models, for various chain lengths, for models without [(a)] and with [(b)] internal friction. Note that $s \equiv t/\tau_1$ for the discrete model and $s \equiv t/\tilde{\tau}_1$ for the continuum model.

written in terms of the cartesian components of $\mathbf{X}_p \equiv [x_p, y_p, z_p]^T$, and $\mathbf{g}_p \equiv [g_p^{(x)}, g_p^{(y)}, g_p^{(z)}]^T$ as

$$\frac{d}{dt} \begin{bmatrix} x_p \\ y_p \\ z_p \end{bmatrix} = - \left(\frac{1}{\tau_p} \right) \begin{bmatrix} x_p \\ y_p \\ z_p \end{bmatrix} + \left(\frac{1}{1 + \theta a_p} \right) \begin{bmatrix} \dot{\gamma} y_p \\ 0 \\ 0 \end{bmatrix} + \begin{bmatrix} g_p^{(x)} \\ g_p^{(y)} \\ g_p^{(z)} \end{bmatrix} \quad (25)$$

Recognizing that Eq. (25) represents a system of three linear stochastic differential equations, we write

$$\frac{dx_p}{dt} + \left(\frac{1}{\tau_p} \right) x_p = \left(\frac{\dot{\gamma}}{1 + \theta a_p} \right) y_p + g_p^{(x)} \quad (26)$$

$$\frac{dy_p}{dt} + \left(\frac{1}{\tau_p} \right) y_p = g_p^{(y)} \quad (27)$$

$$\frac{dz_p}{dt} + \left(\frac{1}{\tau_p} \right) z_p = g_p^{(z)} \quad (28)$$

The equation for x_p depends explicitly on y_p , but y_p is not coupled to x_p . Furthermore, z_p evolves independently of x_p and y_p . The methodology to solve for $y_p(t)$ is identical to that of solving for $z_p(t)$, and consequently, only the steps for the solution of $y_p(t)$ are given. The solution for $x_p(t)$ is dealt with subsequently. In the solution of these three equations [Eqs. (26)-(28)], we closely follow the framework described in detail in Ref. 8.

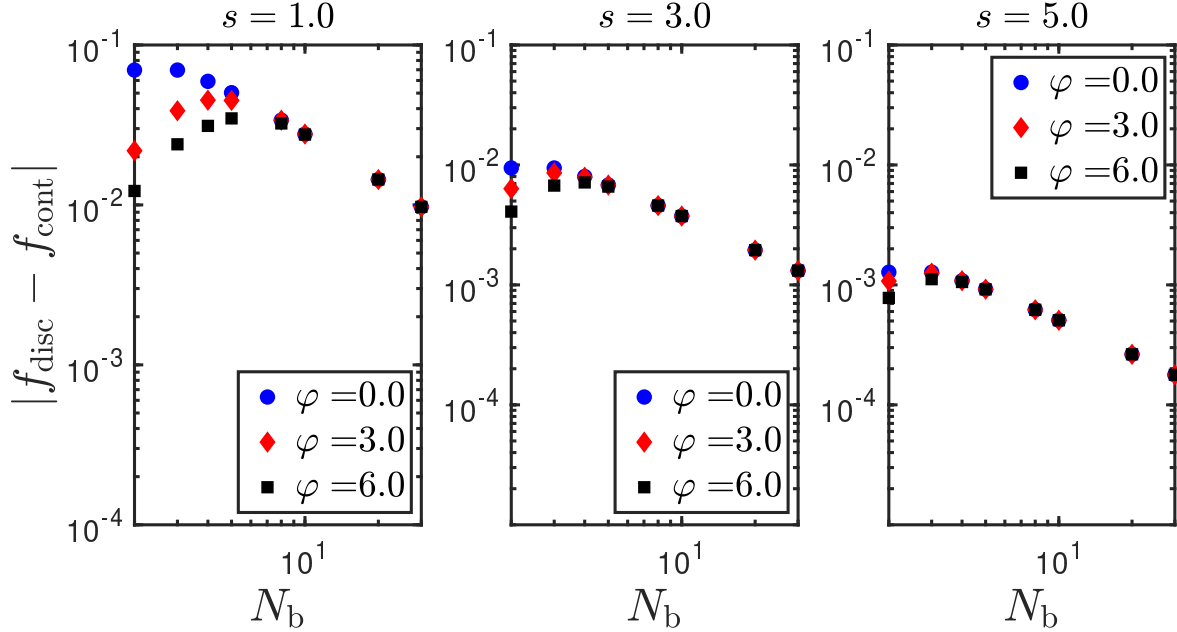


FIG. S3. The absolute value of the difference between the discrete and continuum models at various instances of scaled time, plotted as a function of the chain length, for varying values of the internal friction parameter. Here, f_{disc} represents the normalized autocorrelation for the discrete model at the indicated value of s , and f_{cont} represents the normalized autocorrelation for the continuum model at the same value of s .

We note that

$$\begin{aligned} \langle \mathbf{X}_p(t) \cdot \mathbf{X}_q(t) \rangle &= \langle [x_p(t)\mathbf{e}_x + y_p(t)\mathbf{e}_y + z_p(t)\mathbf{e}_z] \cdot [x_q(t)\mathbf{e}_x + y_q(t)\mathbf{e}_y + z_q(t)\mathbf{e}_z] \rangle \\ &= \langle x_p(t)x_q(t) \rangle + \langle y_p(t)y_q(t) \rangle + \langle z_p(t)z_q(t) \rangle \end{aligned} \quad (29)$$

and our task now involves the computation of the three ensemble-averaged quantities on the RHS of Eq. (29). Starting from Eq. (27), the formal solution for $y_p(t)$ is written as

$$\begin{aligned} y_p(t) &= y_p(0)e^{-t/\tau_p} + \int_0^t dt_1 g_p^{(y)}(t_1) e^{-(t-t_1)/\tau_p} \\ &= y_p(0)e^{-t/\tau_p} + \Delta\mathcal{Y}_p(t) \end{aligned} \quad (30)$$

The moments of $\Delta\mathcal{Y}_p(t)$ are

$$\begin{aligned} \langle \Delta\mathcal{Y}_p(t) \rangle &\equiv \left\langle \int_0^t dt_1 g_p^{(y)}(t_1) e^{-(t-t_1)/\tau_p} \right\rangle \\ &= \int_0^t dt_1 \langle g_p^{(y)}(t_1) \rangle e^{-(t-t_1)/\tau_p} = 0 \end{aligned} \quad (31)$$

and

$$\langle \Delta\mathcal{Y}_p(t)\Delta\mathcal{Y}_q(t) \rangle = \frac{k_B T}{H_p} \delta_{pq} [1 - e^{-2t/\tau_p}] \quad (32)$$

The equal-time correlations of the y - and z - components are identical, and can be derived to be

$$\langle y_p(t)y_q(t) \rangle = \langle z_p(t)z_q(t) \rangle = \frac{k_B T}{H_p} \delta_{pq} \quad (33)$$

Starting from Eq. (26), the formal solution for $x_p(t)$ is written as

$$\begin{aligned} x_p(t) &= x_p(0)e^{-t/\tau_p} + \int_0^t dt_1 g_p^{(x)}(t_1) e^{-(t-t_1)/\tau_p} \\ &\quad + \left(\frac{\dot{\gamma}}{1 + \theta a_p} \right) \int_0^t dt_2 y_p(t_2) e^{-(t-t_2)/\tau_p} \end{aligned} \quad (34)$$

The underlined integral is evaluated as

$$\int_0^t dt_2 y_p(t_2) e^{-(t-t_2)/\tau_p} = t y_p(0) e^{-t/\tau_p} + \int_0^t dt_2 \int_0^{t_2} dt_3 g_p^{(y)}(t_3) e^{-(t-t_3)/\tau_p} \quad (35)$$

with the double-integral solved using the Cauchy formula for repeated integration⁹,

$$\int_0^t dt_2 \int_0^{t_2} dt_3 g_p^{(y)}(t_3) e^{-(t-t_3)/\tau_p} = \frac{1}{(2-1)!} \int_0^t dt' (t-t') g_p^{(y)}(t') e^{-(t-t')/\tau_p}, \quad (36)$$

to obtain the following expression for $x_p(t)$,

$$x_p(t) = e^{-t/\tau_p} \left[x_p(0) + \left(\frac{\dot{\gamma}}{1+\theta a_p} \right) t y_p(0) \right] + \Delta \mathcal{X}_p^{(x)}(t) + \left(\frac{\dot{\gamma}}{1+\theta a_p} \right) \Delta \mathcal{X}_p^{(y)}(t) \quad (37)$$

where

$$\begin{aligned} \Delta \mathcal{X}_p^{(x)}(t) &= \int_0^t dt_1 g_p^{(x)}(t_1) e^{-(t-t_1)/\tau_p} \\ \Delta \mathcal{X}_p^{(y)}(t) &= \int_0^t dt' (t-t') g_p^{(y)}(t') e^{-(t-t')/\tau_p} \end{aligned} \quad (38)$$

The equal-time correlation of the x - component is obtained as

$$\begin{aligned} \langle x_p(t) x_q(t) \rangle &= \left(\frac{k_B T}{H_p} \right) \delta_{pq} e^{-2t/\tau_p} + \underbrace{\langle \Delta \mathcal{X}_p^{(x)}(t) \Delta \mathcal{X}_q^{(x)}(t) \rangle}_{\text{solid-underlined}} + \left(\frac{\dot{\gamma} \tau_p}{1+\theta a_p} \right)^2 \left(\frac{2t}{\tau_p} \right)^2 \left(\frac{k_B T}{4H_p} \right) \delta_{pq} e^{-2t/\tau_p} \\ &+ \left(\frac{\dot{\gamma}}{1+\theta a_p} \right) \left(\frac{\dot{\gamma}}{1+\theta a_q} \right) \underbrace{\langle \Delta \mathcal{X}_p^{(y)}(t) \Delta \mathcal{X}_q^{(y)}(t) \rangle}_{\text{dashed-underlined}} \end{aligned} \quad (39)$$

The solid-underlined term is identical to $\langle \Delta \mathcal{Y}_p(t) \Delta \mathcal{Y}_q(t) \rangle$, and may be obtained from Eq. (32). The dashed underlined term may be simplified as

$$\begin{aligned} \langle \Delta \mathcal{X}_p^{(y)}(t) \Delta \mathcal{X}_q^{(y)}(t) \rangle &= \left\langle \int_0^t dt' (t-t') g_p^{(y)}(t') e^{-(t-t')/\tau_p} \int_0^t dt'' (t-t'') g_p^{(y)}(t'') e^{-(t-t'')/\tau_p} \right\rangle \\ &= \frac{2k_B T}{\zeta_p} \delta_{pq} \int_0^t dt' (t-t')^2 e^{-2(t-t')/\tau_p} \\ &= - \left(\frac{\tau_p}{2} \right) t^2 e^{-2t/\tau_p} + \int_0^t \tau_p (t-t') e^{-2(t-t')/\tau_p} dt' \\ &= - \left(\frac{\tau_p}{2} \right) t^2 e^{-2t/\tau_p} + \left(\frac{\tau_p^2}{2} \right) \int_0^t (t-t') \frac{d}{dt'} \left[e^{-2(t-t')/\tau_p} \right] dt' \\ &= \left(\frac{k_B T}{4H_p} \right) \tau_p^2 \delta_{pq} \left\{ 2 - \left[2 + 2 \left(\frac{2t}{\tau_p} \right) + \left(\frac{2t}{\tau_p} \right)^2 \right] e^{-2t/\tau_p} \right\} \end{aligned} \quad (40)$$

to give

$$\langle x_p(t) x_q(t) \rangle = \left(\frac{k_B T}{H_p} \right) \delta_{pq} + 8 \left(\frac{k_B T}{H_p a_p^2} \right) \delta_{pq} (\lambda_H \dot{\gamma})^2 \left\{ 1 - \left[1 + \left(\frac{2t}{\tau_p} \right) \right] e^{-2t/\tau_p} \right\} \quad (41)$$

Plugging Eqs. (33) and (41) into Eq. (29), the equal-time correlation for the modes is obtained as

$$\langle \mathbf{X}_p(t) \cdot \mathbf{X}_q(t) \rangle = \left(\frac{3k_B T}{H} \right) \left(\frac{1}{a_p} \right) \delta_{pq} \left\{ 1 + \frac{8(\lambda_H \dot{\gamma})^2}{3a_p^2} \left[1 - \left(e^{-2t/\tau_p} \left[1 + \left(\frac{2t}{\tau_p} \right) \right] \right) \right] \right\} \quad (42)$$

Recognizing that the end-to-end vector is given by

$$\mathbf{R}_E(t) = -2\sqrt{\frac{2}{N_b}} \sum_{q:\text{odd}}^{N_b-1} \cos\left(\frac{q\pi}{2N_b}\right) \mathbf{X}_q(t), \quad (43)$$

the expression for $\langle \mathbf{R}_E^2(t) \rangle$ may be written as

$$\langle \mathbf{R}_E^2(t) \rangle = \left(\frac{8}{N_b} \right) \sum_{q:\text{odd}}^{N_b-1} \sum_{p:\text{odd}}^{N_b-1} \cos\left(\frac{p\pi}{2N_b}\right) \cos\left(\frac{q\pi}{2N_b}\right) \langle \mathbf{X}_p(t) \cdot \mathbf{X}_q(t) \rangle \quad (44)$$

Using Eqs. (42) and (44), we get

$$\langle \mathbf{R}_E^2(t) \rangle = \left(\frac{8}{N_b} \right) \left(\frac{3k_B T}{H} \right) \sum_{p:\text{odd}}^{N_b-1} \left(\frac{1}{a_p} \right) \cos^2\left(\frac{p\pi}{2N_b}\right) \left\{ 1 + \frac{8(\lambda_H \dot{\gamma})^2}{3a_p^2} \left[1 - \left(e^{-2t/\tau_p} \left[1 + \left(\frac{2t}{\tau_p} \right) \right] \right) \right] \right\}, \quad (45)$$

which may be written in the dimensionless form as

$$\langle \mathbf{R}_E^{*2}(t^*) \rangle = \left(\frac{24}{N_b} \right) \sum_{p:\text{odd}}^{N_b-1} \left(\frac{1}{a_p} \right) \cos^2\left(\frac{p\pi}{2N_b}\right) \left\{ 1 + \frac{8(\lambda_H \dot{\gamma})^2}{3a_p^2} \left[1 - \left(\exp\left[-\left(\frac{a_p}{1+\theta a_p}\right) \frac{t^*}{2}\right] \left[1 + \left(\frac{a_p}{1+\theta a_p}\right) \frac{t^*}{2}\right] \right) \right] \right\} \quad (46)$$

The steady-state result is obtained by taking the limit $t^* \rightarrow \infty$ in Eq. (46), to give

$$\langle \mathbf{R}_E^{*2} \rangle \equiv \langle \mathbf{R}_E^{*2}(t^* \rightarrow \infty) \rangle = \left(\frac{24}{N_b} \right) \sum_{p:\text{odd}}^{N_b-1} \left(\frac{1}{a_p} \right) \cos^2\left(\frac{p\pi}{2N_b}\right) \left\{ 1 + \frac{8(\lambda_H \dot{\gamma})^2}{3a_p^2} \right\} \quad (47)$$

In the limit of large N_b , Eq. (47) is found to agree with Eq. (10) of Ref. 10, which is the result for a continuum model of a Rouse chain in shear flow. Scaling Eq. (46) by the mean-squared end-to-end vector gives

$$\begin{aligned} \frac{\langle \mathbf{R}_E^{*2}(t^*) \rangle}{\langle \mathbf{R}_E^{*2} \rangle_{\text{eq}}} &= \left[\frac{8}{N_b(N_b-1)} \right] \sum_{p:\text{odd}}^{N_b-1} \left(\frac{1}{a_p} \right) \cos^2\left(\frac{p\pi}{2N_b}\right) \\ &\times \left\{ 1 + \frac{8(\lambda_H \dot{\gamma})^2}{3a_p^2} \left[1 - \left(\exp\left[-\left(\frac{a_p}{1+\theta a_p}\right) \frac{t^*}{2}\right] \left[1 + \left(\frac{a_p}{1+\theta a_p}\right) \frac{t^*}{2}\right] \right) \right] \right\} \end{aligned} \quad (48)$$

III. EQUIVALENCE BETWEEN DISCRETE RIF AND THE PRAVERAGED INTERNAL FRICTION MODEL

A. Derivation of governing equation

We consider a freely-draining chain of N_b massless beads where the neighbors are connected by means of a spring in parallel with a dashpot whose damping coefficient is K . The locations of the beads are given by $\{\mathbf{r}_1, \mathbf{r}_2, \dots, \mathbf{r}_{N_b}\}$, and the connector vector between adjacent beads is denoted by $\mathbf{Q}_j = \mathbf{r}_{j+1} - \mathbf{r}_j$, where $j \in [1, N]$. We assume an overdamped system that has equilibrated in momentum space, and the instantaneous normalized configuration distribution function for the chain is given by $\Psi \equiv \Psi(\mathbf{r}_1, \mathbf{r}_2, \dots, \mathbf{r}_{N_b}, t) = (1/\mathcal{Z}) \exp[-\phi/k_B T]$, where ϕ denotes the intramolecular potential energy stored in the springs joining the beads and $\mathcal{Z} = \int \exp[-\phi/k_B T] d\mathbf{Q}_1 d\mathbf{Q}_2 \dots d\mathbf{Q}_N$. It is noted that Ψ remains unmodified by the inclusion of internal viscosity. Using the principles of polymer kinetic theory^{2,4,11}, the equation of motion for the momentum-averaged velocity of the j^{th} connector vector may be

derived to be

$$\begin{aligned} \llbracket \dot{\mathbf{Q}}_j \rrbracket &= \boldsymbol{\kappa} \cdot \mathbf{Q}_j - \frac{1}{\zeta} \sum_k A_{jk} \left(k_B T \frac{\partial \ln \Psi}{\partial \mathbf{Q}_k} + \frac{\partial \phi}{\partial \mathbf{Q}_k} \right. \\ &\quad \left. + K \frac{\mathbf{Q}_k \mathbf{Q}_k}{Q_k^2} \cdot \llbracket \dot{\mathbf{Q}}_k \rrbracket \right) \end{aligned} \quad (49)$$

where

$$A_{jk} = \begin{cases} 2; & j = k \\ -1; & |j - k| = 1 \\ 0; & \text{otherwise} \end{cases} \quad (50)$$

Clearly, the equation for the j^{th} connector-vector velocity is coupled to that of its nearest neighbors, which precludes not only the naive substitution of Eq. (49) into an equation of continuity in Ψ , but also the derivation of the Fokker-Planck equation and the governing set of stochastic differential equations for the system, for all but the simplest case of a dumbbell ($N = 1$). Manke and Williams¹² proposed a three-step iterative substitution methodology (details given below) for the

decoupling of the connector vector velocities, and derived semi-analytical approximate expressions for the linear-viscoelastic properties^{12,13} of chains with internal friction. In our recent work [Ref. 4, under review], we have expanded the scope of the Manke and Williams decoupling methodology to obtain the governing set of exact stochastic differential equations for a Rouse chain with fluctuating internal viscosity that are valid both at equilibrium and in the presence of a flow profile. The approximate solutions derived by Manke and Williams compare excellently against simulation results obtained by numerically integrating the exact stochastic differential equations using Brownian dynamics (BD) simulations. We have also presented, for the first time, data on the steady-shear viscometric functions for Rouse chains with fluctuating internal friction, for the general case of $N > 1$. The same methodology is applied to solve

for the governing stochastic differential equations of a Rouse chain with preaveraged internal viscosity.

As detailed in the discussion surrounding Eq. (5) in the main text, the preaveraging approximation entails a replacement of the underlined term in Eq. (49) by its average evaluated with respect to the equilibrium distribution function of a Rouse chain, which is $(\delta/3)$. Therefore, for a chain with preaveraged internal viscosity, Eq. (49) reduces to

$$\begin{aligned} \llbracket \dot{\mathbf{Q}}_j \rrbracket = & \boldsymbol{\kappa} \cdot \mathbf{Q}_j - \frac{1}{\zeta} \sum_k A_{jk} \left(k_B T \frac{\partial \ln \Psi}{\partial \mathbf{Q}_k} + \frac{\partial \phi}{\partial \mathbf{Q}_k} \right. \\ & \left. + \frac{K}{3} \llbracket \dot{\mathbf{Q}}_k \rrbracket \right) \end{aligned} \quad (51)$$

which may be simplified, using $\theta = (K/3\zeta)$, to give

$$\begin{aligned} \llbracket \dot{\mathbf{Q}}_j \rrbracket = & \left(\frac{1}{1+2\theta} \right) (\boldsymbol{\kappa} \cdot \mathbf{Q}_k) - \left(\frac{k_B T}{\zeta} \right) \left(\frac{1}{1+2\theta} \right) \left[-\frac{\partial \ln \Psi}{\partial \mathbf{Q}_{k-1}} + 2 \frac{\partial \ln \Psi}{\partial \mathbf{Q}_k} - \frac{\partial \ln \Psi}{\partial \mathbf{Q}_{k+1}} \right] \\ & - \left(\frac{1}{\zeta} \right) \left(\frac{1}{1+2\theta} \right) \left[-\frac{\partial \phi}{\partial \mathbf{Q}_{k-1}} + 2 \frac{\partial \phi}{\partial \mathbf{Q}_k} - \frac{\partial \phi}{\partial \mathbf{Q}_{k+1}} \right] + \left(\frac{\theta}{1+2\theta} \right) \llbracket \dot{\mathbf{Q}}_{j-1} \rrbracket + \left(\frac{\theta}{1+2\theta} \right) \llbracket \dot{\mathbf{Q}}_{j+1} \rrbracket \end{aligned} \quad (52)$$

An ensuing simplicity of the preaveraging approximation is that Eq. (52) may directly be subjected to the iterative-substitution-based decoupling methodology, unlike the case with fluctuations where the expression for $\mathbf{Q}_k \cdot \llbracket \dot{\mathbf{Q}}_k \rrbracket / Q_k^2$ must first be decoupled before obtaining the desired expression for $\llbracket \dot{\mathbf{Q}}_k \rrbracket$.

Firstly, in the forward substitution step, the expression for $\llbracket \dot{\mathbf{Q}}_j \rrbracket$ is substituted into that for $\llbracket \dot{\mathbf{Q}}_{j+1} \rrbracket$, iteratively, starting from $j = 1$ until $j = (N - 1)$. This results in the following general expression,

$$\begin{aligned} (1 - M_k) \llbracket \dot{\mathbf{Q}}_k \rrbracket = & \left(\frac{\theta}{1+2\theta} \right) \llbracket \dot{\mathbf{Q}}_{k+1} \rrbracket + \left(\frac{1}{1+2\theta} \right) \sum_{l=1}^k \Gamma_l^{(k)} (\boldsymbol{\kappa} \cdot \mathbf{Q}_l) + (1 - \delta_{kN}) \left(\frac{k_B T}{\zeta} \right) \left(\frac{1}{1+2\theta} \right) \left(\frac{\partial \ln \Psi}{\partial \mathbf{Q}_{k+1}} \right) \\ & + (1 - \delta_{kN}) \left(\frac{1}{\zeta} \right) \left(\frac{1}{1+2\theta} \right) \left(\frac{\partial \phi}{\partial \mathbf{Q}_{k+1}} \right) - \left(\frac{k_B T}{\zeta} \right) \left(\frac{1}{1+2\theta} \right) \sum_{l=1}^k E_l^{(k)} \left(\frac{\partial \ln \Psi}{\partial \mathbf{Q}_l} \right) - \left(\frac{1}{\zeta} \right) \left(\frac{1}{1+2\theta} \right) \sum_{l=1}^k E_l^{(k)} \left(\frac{\partial \phi}{\partial \mathbf{Q}_l} \right) \end{aligned} \quad (53)$$

where the explicit dependence of $\llbracket \dot{\mathbf{Q}}_k \rrbracket$ on $\llbracket \dot{\mathbf{Q}}_{k-1} \rrbracket$ has been removed and the following definitions apply

$$M_k = \left(\frac{\theta}{1+2\theta} \right)^2 \left(\frac{1}{1 - M_{k-1}} \right); \text{ with } M_1 = 0 \quad (54)$$

$$\Gamma_l^{(k)} = \left(\frac{\theta}{1+2\theta} \right)^{k-l} \prod_{i=l}^{k-1} \left(\frac{1}{1 - M_i} \right) \quad (55)$$

$$E_l^{(k)} = 2\Gamma_l^{(k)} - \Gamma_{l-1}^{(k)} - \Gamma_{l+1}^{(k)} \quad (56)$$

Next, in the backward substitution step, the expression for $\llbracket \dot{\mathbf{Q}}_j \rrbracket$ is substituted into that for $\llbracket \dot{\mathbf{Q}}_{j-1} \rrbracket$, iteratively,

starting from $j = N$ until $j = 2$. This results in the following general expression,

$$\begin{aligned} \llbracket \dot{\mathbf{Q}}_k \rrbracket &= \left(\frac{\theta}{1+2\theta} \right) \left(\frac{1}{1-P_k} \right) \llbracket \dot{\mathbf{Q}}_{k-1} \rrbracket + \left(\frac{1}{1+2\theta} \right) \sum_{l=k}^N \tilde{\rho}_l^{(k)} (\boldsymbol{\kappa} \cdot \mathbf{Q}_l) + \left(\frac{k_B T}{\zeta} \right) \left(\frac{1}{1+2\theta} \right) \left(\frac{1}{1-P_k} \right) \left(\frac{\partial \ln \Psi}{\partial \mathbf{Q}_{k-1}} \right) \\ &+ \left(\frac{1}{\zeta} \right) \left(\frac{1}{1+2\theta} \right) \left(\frac{1}{1-P_k} \right) \left(\frac{\partial \phi}{\partial \mathbf{Q}_{k-1}} \right) - \left(\frac{k_B T}{\zeta} \right) \left(\frac{1}{1+2\theta} \right) \sum_{l=k}^N \tilde{G}_l^{(k)} \left(\frac{\partial \ln \Psi}{\partial \mathbf{Q}_l} \right) - \left(\frac{1}{\zeta} \right) \left(\frac{1}{1+2\theta} \right) \sum_{l=k}^N \tilde{G}_l^{(k)} \left(\frac{\partial \phi}{\partial \mathbf{Q}_l} \right) \end{aligned} \quad (57)$$

where the explicit dependence of $\llbracket \dot{\mathbf{Q}}_k \rrbracket$ on $\llbracket \dot{\mathbf{Q}}_{k+1} \rrbracket$ has been removed and the following definitions apply

$$P_k = \left(\frac{\theta}{1+2\theta} \right)^2 \left(\frac{1}{1-P_{k+1}} \right); \text{ with } P_N = 0. \quad (58)$$

$$\tilde{\rho}_l^{(k)} = \left(\frac{\theta}{1+2\theta} \right)^{l-k} \prod_{i=k}^l \left(\frac{1}{1-P_i} \right) \quad (59)$$

The quantity $\tilde{G}_l^{(k)}$ appearing in Eq. (57) is constructed using a slightly elaborate procedure. It is useful to first consider the Rouse matrix, \mathbf{A} [defined as in Eq. (50)], of size $\Upsilon \times \Upsilon$, where $\Upsilon = (N - k) + 1$, and the intermediate quantity,

$$\tilde{\mathbf{Y}}_s^{(k)} = \left(\frac{\theta}{1+2\theta} \right)^{s-1} \left[\prod_{i=k}^{k+s-1} \left(\frac{1}{1-P_i} \right) \right] \quad (60)$$

which is then used to populate a matrix, $\hat{\boldsymbol{\Theta}}^{(k)}$, of size $\Upsilon \times \Upsilon$ that has the following structure

$$\hat{\boldsymbol{\Theta}}^{(k)} = \begin{pmatrix} \tilde{\mathbf{Y}}_1^{(k)} & \tilde{\mathbf{Y}}_1^{(k)} & 0 & \cdots & & \\ \tilde{\mathbf{Y}}_2^{(k)} & \tilde{\mathbf{Y}}_2^{(k)} & \tilde{\mathbf{Y}}_2^{(k)} & 0 & \cdots & \\ 0 & \tilde{\mathbf{Y}}_3^{(k)} & \tilde{\mathbf{Y}}_3^{(k)} & \tilde{\mathbf{Y}}_3^{(k)} & \cdots & \\ \vdots & \vdots & \vdots & & & \\ 0 & 0 & \cdots & \tilde{\mathbf{Y}}_\Upsilon^{(k)} & \tilde{\mathbf{Y}}_\Upsilon^{(k)} & \end{pmatrix} \quad (61)$$

We next consider the matrix $\mathbf{Z}^{(k)}$ constructed from

\mathbf{A} [see Eq. (50)] and $\hat{\boldsymbol{\Theta}}^{(k)}$, such that $\mathbf{Z}^{(k)} = \mathbf{A} \cdot \hat{\boldsymbol{\Theta}}^{(k)}$. Now, $\tilde{G}_{k+m}^{(k)}$ is defined as the $(m+1)^{\text{th}}$ diagonal element of $\mathbf{Z}^{(k)}$. As the final step of the decoupling procedure, a change of variable, $k \rightarrow (k+1)$, is performed in Eq. (57), and the resulting expression is substituted into the equation derived from the forward substitution step [Eq. (53)]. The decoupled expression for $\llbracket \dot{\mathbf{Q}}_k \rrbracket$ is finally obtained as

$$\llbracket \dot{\mathbf{Q}}_k \rrbracket = \left(\frac{1}{1+2\theta} \right) \sum_{l=1}^N \Lambda_{kl} (\boldsymbol{\kappa} \cdot \mathbf{Q}_l) - \left(\frac{1}{\zeta} \right) \left(\frac{1}{1+2\theta} \right) \sum_{l=1}^N J_{kl} \left(\frac{\partial \phi}{\partial \mathbf{Q}_l} \right) - \left(\frac{k_B T}{\zeta} \right) \left(\frac{1}{1+2\theta} \right) \sum_{l=1}^N J_{kl} \left(\frac{\partial \ln \Psi}{\partial \mathbf{Q}_l} \right) \quad (62)$$

In defining Eqs. (55), (59), and (60), we have adopted the convention $0^0 = 1$, i.e., when $\theta = 0$, $\Gamma_k^{(k)} = \tilde{\rho}_k^{(k)} = \tilde{\mathbf{Y}}_1^{(k)} = 1$. The matrix elements, Λ_{kl} , and J_{kl} , each of size $N \times N$, are defined as

$$\Lambda_{kl} = \left(\frac{1}{1-M_k-P_k} \right) \hat{\Lambda}_{kl}; \quad J_{kl} = \left(\frac{1}{1-M_k-P_k} \right) \hat{J}_{kl} \quad (63)$$

with

$$\hat{\Lambda}_{kl} = \begin{cases} \Gamma_l^{(k)}; & l < k \\ 1; & l = k \\ \left(\frac{\theta}{1+2\theta} \right) \tilde{\rho}_l^{(k+1)}; & l > k \end{cases} \quad (64)$$

and

$$\widehat{\mathbf{J}}_{kl} = \begin{cases} E_l^{(k)}; & l < k \\ E_l^{(k)} - (1 - \delta_{kN}) \left(\frac{1}{1 - P_{k+1}} \right) \left(\frac{\theta}{1 + 2\theta} \right); & l = k \\ (1 - \delta_{kN}) \left[\left(\frac{\theta}{1 + 2\theta} \right) \widetilde{G}_l^{(k+1)} - 1 \right]; & l = k + 1 \\ \left(\frac{\theta}{1 + 2\theta} \right) \widetilde{G}_l^{(k+1)}; & l > (k + 1) \end{cases} \quad (65)$$

The procedure for the construction of $\widetilde{G}_l^{(k+1)}$ which appears in Eq. (65) is fairly similar to that described in Eq. (61) for the construction of $\widetilde{G}_l^{(k)}$, with the only caveat that the size of the block matrices, \mathbf{A} and the $\widehat{\Theta}^{(k+1)}$, remain $\Upsilon \times \Upsilon$, where $\Upsilon = (N - k) + 1$.

Another point of difference between the preaveraged IV model and the fluctuating IV one is that for the former, the quantities $\{M_k, P_k, \Gamma_l^{(k)}, E_l^{(k)}, \widetilde{\rho}_l^{(k)}, \widetilde{Y}_s^{(k)}, \widetilde{G}_l^{(k)}, \Lambda_{kl}, J_{kl}\}$ are functions only of the internal friction parameter θ , and not dependent on the chain configuration. In the fluctuating IV model, however, these quantities are functions of both the internal friction parameter, and the chain configuration.

As the next step, the expression for $[\dot{\mathbf{Q}}_k]$ will be substituted into the equation of continuity, recognizing that the homogeneous flow profile allows one to write the continuity equation solely in terms of the relative coordinates, \mathbf{Q}_k . This means that the distribution function $\Psi(\mathbf{r}_c, \mathbf{Q}_1, \mathbf{Q}_2, \dots, \mathbf{Q}_N)$ can be replaced by $\psi(\mathbf{Q}_1, \mathbf{Q}_2, \dots, \mathbf{Q}_N)$, and we have

$$\begin{aligned} \frac{\partial \psi}{\partial t} &= - \sum_{k=1}^N \frac{\partial}{\partial \mathbf{Q}_k} \cdot \left\{ [\dot{\mathbf{Q}}_k] \psi \right\} \\ &= - \sum_{k=1}^N \frac{\partial}{\partial \mathbf{Q}_k} \cdot \left\{ \left[\left(\frac{1}{1 + 2\theta} \right) \sum_{l=1}^N \Lambda_{kl} \cdot (\boldsymbol{\kappa} \cdot \mathbf{Q}_l) \right. \right. \\ &\quad \left. \left. - \left(\frac{1}{\zeta} \right) \left(\frac{1}{1 + 2\theta} \right) \sum_{l=1}^N \mathbf{J}_{kl} \cdot \left(\frac{\partial \phi}{\partial \mathbf{Q}_l} \right) \right] \psi \right\} \\ &\quad + \left(\frac{k_B T}{\zeta} \right) \left(\frac{1}{1 + 2\theta} \right) \sum_{k=1}^N \sum_{l=1}^N \frac{\partial}{\partial \mathbf{Q}_k} \cdot \left[\mathbf{J}_{kl} \cdot \frac{\partial \psi}{\partial \mathbf{Q}_l} \right] \end{aligned} \quad (66)$$

where $\mathbf{J}_{kl} = J_{kl} \boldsymbol{\delta}$, and $\Lambda_{kl} = \Lambda_{kl} \boldsymbol{\delta}$. Since \mathbf{J}_{kl} is composed entirely of constant coefficients that are independent of the stochastic variables \mathbf{Q}_k , it is divergence-free, and the noise term may be rewritten, giving the follow-

ing Fokker-Planck equation

$$\begin{aligned} \frac{\partial \psi}{\partial t} &= - \sum_{k=1}^N \frac{\partial}{\partial \mathbf{Q}_k} \cdot \left\{ \left[\left(\frac{1}{1 + 2\theta} \right) \sum_{l=1}^N \Lambda_{kl} \cdot (\boldsymbol{\kappa} \cdot \mathbf{Q}_l) \right. \right. \\ &\quad \left. \left. - \left(\frac{1}{\zeta} \right) \left(\frac{1}{1 + 2\theta} \right) \sum_{l=1}^N \mathbf{J}_{kl} \cdot \left(\frac{\partial \phi}{\partial \mathbf{Q}_l} \right) \right] \psi \right\} \\ &\quad + \left(\frac{k_B T}{\zeta} \right) \left(\frac{1}{1 + 2\theta} \right) \sum_{k=1}^N \sum_{l=1}^N \frac{\partial}{\partial \mathbf{Q}_k} \frac{\partial}{\partial \mathbf{Q}_l} : [\mathbf{J}_{kl} \psi] \end{aligned} \quad (67)$$

where we have implicitly used the fact that $\mathbf{J}_{kl}^T = J_{kl} \boldsymbol{\delta}^T = \mathbf{J}_{kl}$, and $J_{kl} = J_{lk}$. Noting that $\mathbf{F}_l^{(\phi)} \equiv (\partial \phi / \partial \mathbf{Q}_l) = H \mathbf{Q}_l$ for Hookean springs, the stochastic differential equation may be written, using the Itô interpretation³ of Eq. (67), as

$$\begin{aligned} d\mathbf{Q}_k &= \left(\frac{1}{1 + 2\theta} \right) \left[\sum_{l=1}^N \Lambda_{kl} (\boldsymbol{\kappa} \cdot \mathbf{Q}_l) \right. \\ &\quad \left. - \left(\frac{H}{\zeta} \right) \sum_{l=1}^N J_{kl} \mathbf{Q}_l \right] dt + \sqrt{\frac{2k_B T}{\zeta(1 + 2\theta)}} \sum_{l=1}^N B_{kl} d\mathbf{W}_l \end{aligned} \quad (68)$$

where

$$\sum_{j=1}^N B_{kj} B_{lj} = J_{kl} \quad (69)$$

Eq. (68) is integrated numerically using the simple Euler discretization³ method, with a time-step width of $\Delta t^* = 10^{-3}$. Averages are evaluated over an ensemble of $\mathcal{O}(10^5)$ trajectories. The Langevin equation corresponding to Eq. (68) is given by

$$\begin{aligned} \frac{d\mathbf{Q}_k}{dt} &= \left(\frac{1}{1 + 2\theta} \right) \left[\sum_{l=1}^N \Lambda_{kl} (\boldsymbol{\kappa} \cdot \mathbf{Q}_l) - \left(\frac{H}{\zeta} \right) \sum_{l=1}^N J_{kl} \mathbf{Q}_l \right] \\ &\quad + \sqrt{\frac{2k_B T}{\zeta(1 + 2\theta)}} \sum_{l=1}^N B_{kl} \mathbf{f}_l(t) \end{aligned} \quad (70)$$

where

$$\begin{aligned}\langle \mathbf{f}_i(t) \rangle &= 0 \\ \langle \mathbf{f}_i(t) \mathbf{f}_m(t') \rangle &= \delta_{mi} \delta \delta(t-t') \\ \langle \mathbf{f}_i(t) \cdot \mathbf{f}_m(t') \rangle &= 3 \delta_{mi} \delta(t-t')\end{aligned}\quad (71)$$

Semi-analytical solutions to Eq. (70) at equilibrium and in the presence of shear flow are presented below.

B. Normal mode analysis at equilibrium

To obtain the correlation of the end-to-end vector for a Rouse chain with preaveraged internal friction, we set $\kappa = 0$ in Eq. (70) and obtain the governing Langevin

equation as

$$\begin{aligned}\frac{d\mathbf{Q}_k}{dt} &= - \left[\frac{H}{\zeta(1+2\theta)} \right] \sum_{l=1}^N J_{kl} \mathbf{Q}_l \\ &+ \sqrt{\frac{2k_B T}{\zeta(1+2\theta)}} \sum_{l=1}^N B_{kl} \mathbf{f}_l(t)\end{aligned}\quad (72)$$

This equation is converted into normal mode coordinates by means of the transformation $\mathbf{Q}'_j = \sum_m \Pi_{mj} \mathbf{Q}_m$, where the orthogonalizing matrix $\mathbf{\Pi}$ satisfies the following properties

$$\begin{aligned}\sum_{k=1}^N \Pi_{kj} \Pi_{kl} &= \delta_{jl} = \sum_{n=1}^N \Pi_{jn} \Pi_{ln} \\ \sum_{l=1}^N \sum_{n=1}^N \Pi_{lj} J_{ln} \Pi_{nk} &= \tilde{a}_j \delta_{jk}\end{aligned}\quad (73)$$

and must be determined numerically. In Eq. (73), the \tilde{a}_j represent the eigenvalues of \mathbf{J} .

The governing equation for the normal coordinates is given as

$$\frac{d\mathbf{Q}'_m}{dt} = - \left[\frac{H \tilde{a}_m}{\zeta(1+2\theta)} \right] \mathbf{Q}'_m + \sqrt{\frac{2k_B T}{\zeta(1+2\theta)}} \sum_k \sum_l \Pi_{km} B_{kl} \mathbf{f}_l(t)\quad (74)$$

whose formal solution may be written as

$$\mathbf{Q}'_m(t) = \mathbf{Q}'_m(0) e^{-t/\hat{\tau}_m} + \sqrt{\frac{2k_B T}{\zeta(1+2\theta)}} \int_0^t dt_1 \left[\sum_k \sum_l \Pi_{km} B_{kl} \mathbf{f}_l(t_1) \right] e^{-(t-t_1)/\hat{\tau}_m}\quad (75)$$

where $\hat{\tau}_m = \zeta(1+2\theta)/H\tilde{a}_m$. The autocorrelation of the normal modes may be derived to be

$$\langle \mathbf{Q}'_p(0) \cdot \mathbf{Q}'_m(t) \rangle = \frac{3k_B T}{H} \delta_{pm} e^{-t/\hat{\tau}_p}\quad (76)$$

Recognizing that

$$\langle \mathbf{R}_E(0) \cdot \mathbf{R}_E(t) \rangle = \sum_{i,m,j,p} \Pi_{im} \Pi_{jp} \langle \mathbf{Q}'_p(0) \cdot \mathbf{Q}'_m(t) \rangle\quad (77)$$

and

$$\frac{t}{\hat{\tau}_p} \equiv \left[\frac{H \tilde{a}_p t}{\zeta(1+2\theta)} \right] = \left[\frac{H \tilde{a}_p t}{4H \lambda_H (1+2\theta)} \right] = \left(\frac{1}{4} \right) \left(\frac{\tilde{a}_p}{1+2\theta} \right) \left(\frac{t}{\lambda_H} \right) = \left(\frac{\tilde{a}_p}{1+2\theta} \right) \frac{t^*}{4}\quad (78)$$

the normalized autocorrelation of the end-to-end vector in dimensionless time units may be written as

$$\frac{\langle \mathbf{R}_E^*(0) \cdot \mathbf{R}_E^*(t^*) \rangle}{\langle \mathbf{R}_E^{*2}(0) \rangle} = \left[\frac{1}{N_b - 1} \right] \sum_{i,j,p}^{N_b-1} \Pi_{ip} \Pi_{jp} \exp \left[- \left(\frac{\tilde{a}_p}{1+2\theta} \right) \frac{t^*}{4} \right]\quad (79)$$

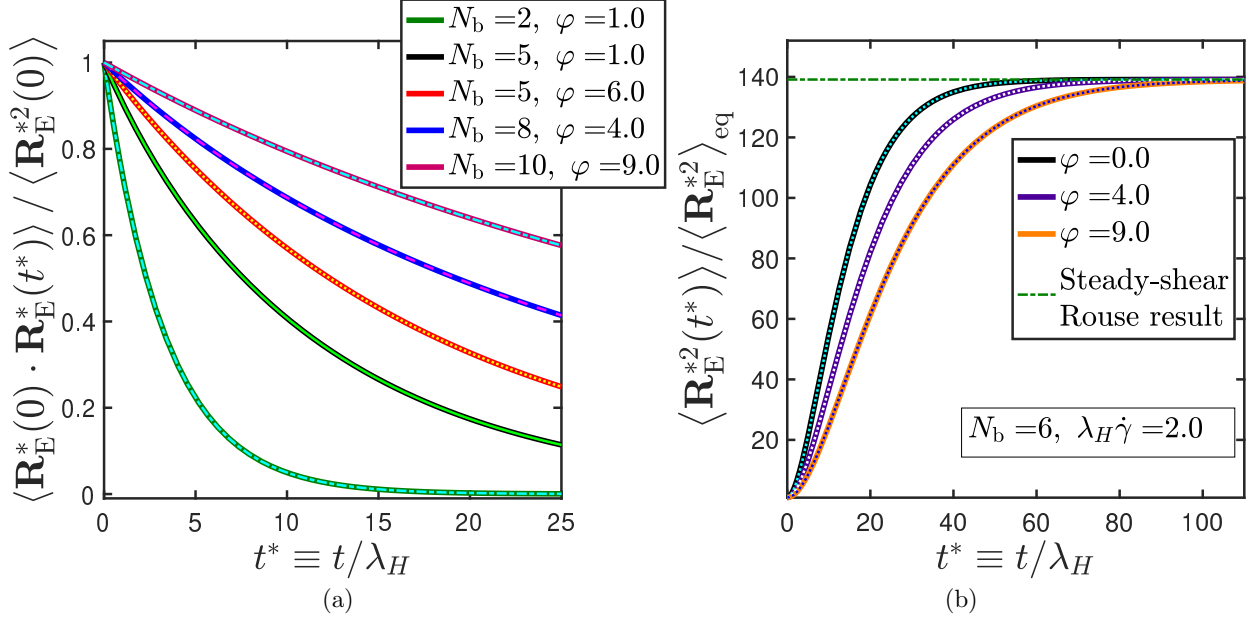


FIG. S4. A comparison of the results for the (a) normalized autocorrelation and (b) transient evolution of the mean-squared end-to-end vector predicted by the discrete RIF model and the preaveraged IV model derived using the principles of polymer kinetic theory. Each legend entry corresponds to two lines: the thicker lines represents the discrete RIF results [Eq. 17 in (a) and Eq. (48) in (b)], while the thinner lines represents semi-analytical solutions for the preaveraged IV model [Eq. 79 in (a) and Eq. (86) in (b)].

C. Normal mode analysis in shear flow

The governing Langevin equation for a Rouse chain with preaveraged internal friction in shear flow is written as

$$\frac{d\mathbf{Q}_k}{dt} = \left(\frac{1}{1+2\theta} \right) \left[\sum_{l=1}^N \Lambda_{kl} (\boldsymbol{\kappa} \cdot \mathbf{Q}_l) - \frac{H}{\zeta} J_{kl} \mathbf{Q}_l \right] + \sqrt{\frac{2k_B T}{\zeta(1+2\theta)}} \sum_{l=1}^N B_{kl} \mathbf{f}_l(t) \quad (80)$$

Eq. (80) is transformed into normal coordinates using the orthogonalizing matrix introduced in Eq. (73). It is assumed that the same matrix also orthogonalizes Λ_{kl} , such that

$$\sum_{l=1}^N \sum_{k=1}^N \Pi_{km} \Lambda_{kl} \Pi_{lq} = \tilde{b}_m \delta_{mq} \quad (81)$$

The quality of this assumption is found to be excellent, based on several test cases. The governing equation in normal coordinates is derived to be

$$\frac{d\mathbf{Q}'_m}{dt} = \left(\frac{\tilde{b}_m}{1+2\theta} \right) \boldsymbol{\kappa} \cdot \mathbf{Q}'_m - \left[\frac{H \tilde{a}_m}{\zeta(1+2\theta)} \right] \mathbf{Q}'_m + \sqrt{\frac{2k_B T}{\zeta(1+2\theta)}} \sum_k \sum_l \Pi_{km} B_{kl} \mathbf{f}_l(t) \quad (82)$$

Following a procedure identical to that described in Sec. IIB, the correlation between the Cartesian components of the normal modes can be derived to be

$$\begin{aligned} \langle Q'_p(x)(t) Q'_q(x)(t) \rangle &= \left(\frac{k_B T}{H} \right) \delta_{pq} + 8 \left(\frac{k_B T}{H} \right) \delta_{pq} \left(\frac{\tilde{b}_q}{\tilde{a}_q} \right)^2 (\lambda_H \dot{\gamma})^2 \left[1 - \left(e^{-2t/\tilde{\tau}_q} \left[1 + \left(\frac{2t}{\tilde{\tau}_q} \right) \right] \right) \right] \\ \langle Q'_p(y)(t) Q'_q(y)(t) \rangle &= \langle Q'_p(z)(t) Q'_q(z)(t) \rangle = \left(\frac{k_B T}{H} \right) \delta_{pq} \\ \langle Q'_p(x)(t) Q'_q(y)(t) \rangle &= \left(\frac{k_B T}{H} \right) \delta_{pq} (\lambda_H \dot{\gamma}) I_q(t) \end{aligned} \quad (83)$$

where

$$I_q(t) = 2 \left(\frac{\tilde{b}_q}{\tilde{a}_q} \right) \left[1 - e^{-2t/\tilde{\tau}_q} \right]. \quad (84)$$

The equal-time correlation of the normal modes is subsequently obtained as

$$\langle \mathbf{Q}'_p(t) \cdot \mathbf{Q}'_q(t) \rangle = \left(\frac{3k_B T}{H} \right) \delta_{pq} \left\{ 1 + \frac{8(\lambda_H \dot{\gamma})^2}{3} \left(\frac{\tilde{b}_p}{\tilde{a}_p} \right)^2 \left[1 - \left(e^{-2t/\tilde{\tau}_p} \left[1 + \left(\frac{2t}{\tilde{\tau}_p} \right) \right] \right) \right] \right\}, \quad (85)$$

and the time evolution of the normalized mean-squared end-to-end distance may then be derived to be

$$\begin{aligned} \frac{\langle \mathbf{R}_E^{*2}(t^*) \rangle}{\langle \mathbf{R}_E^{*2} \rangle_{\text{eq}}} &= \left[\frac{1}{N_b - 1} \right] \sum_{i,j,p}^{N_b-1} \Pi_{ip} \Pi_{jp} \left\{ 1 + \frac{8(\lambda_H \dot{\gamma})^2}{3} \left(\frac{\tilde{b}_p}{\tilde{a}_p} \right)^2 \left[1 - \left(\exp \left[- \left(\frac{\tilde{a}_p}{1 + 2\theta} \right) \frac{t^*}{2} \right] \right. \right. \right. \\ &\quad \left. \left. \left. \times \left[1 + \left(\frac{\tilde{a}_p}{1 + 2\theta} \right) \frac{t^*}{2} \right] \right) \right] \right\} \end{aligned} \quad (86)$$

In Fig. 1 of the main text, the equivalence between the discrete RIF model and the preaveraged IV model is established by comparison of the analytical predictions of the discrete RIF model against BD simulation data obtained by numerically integrating the stochastic differential equation for the preaveraged IV model [Eq. (68)]. In Fig. S4, predictions of the discrete RIF model are compared against the semi-analytical solutions for the preaveraged IV model, and an excellent agreement is observed.

We have therefore established that: (a) the discrete RIF model and the preaveraged IV model are equivalent, and (b) the preaveraged model may be solved

for observables at equilibrium and in simple shear flow using either BD simulations to integrate the governing stochastic differential equation [Eq. (68)] or a semi-analytical approach involving the normal-mode decomposition of the governing Langevin equation [Eq. (70)].

For models with fluctuating IV, it is known¹⁴ that the Kramers expression for the stress tensor is thermodynamically inconsistent, and the Giesekus expression is recommended instead. We have adopted this choice in our recent work⁴ on Rouse chains with fluctuating internal friction. In the absence of any discussion surrounding the viscometric functions of chains with preaveraged internal friction, we have used the Giesekus expression², as follows

$$\boldsymbol{\tau}_p = \frac{n_p \zeta}{2} \left\langle \sum_{j=1}^N \sum_{k=1}^N \mathcal{C}_{jk} \mathbf{Q}_j \mathbf{Q}_k \right\rangle_{(1)} = \frac{n_p \zeta}{2} \left[\frac{d}{dt} \left\langle \sum_{j,k} \mathcal{C}_{jk} \mathbf{Q}_j \mathbf{Q}_k \right\rangle - \boldsymbol{\kappa} \cdot \left\langle \sum_{j,k} \mathcal{C}_{jk} \mathbf{Q}_j \mathbf{Q}_k \right\rangle - \left\langle \sum_{j,k} \mathcal{C}_{jk} \mathbf{Q}_j \mathbf{Q}_k \right\rangle \cdot \boldsymbol{\kappa}^T \right] \quad (87)$$

with \mathcal{C}_{jk} denoting the Kramers matrix constructed as²

$$\mathcal{C}_{jk} = \begin{cases} j(N_b - k)/N_b; & j \leq k \\ k(N_b - j)/N_b; & k \leq j \end{cases} \quad (88)$$

Upon simplification, the stress tensor expression is written as

$$\begin{aligned} \boldsymbol{\tau}_p &= n_p k_B T \left[\left(\frac{1}{1 + 2\theta} \right) \text{tr}(\boldsymbol{\mathcal{L}}) \boldsymbol{\delta} - \frac{n_p H}{2} \left[\left(\frac{1}{1 + 2\theta} \right) \sum_{m,n} \mathcal{L}_{mn} [\langle \mathbf{Q}_m \mathbf{Q}_n \rangle + \langle \mathbf{Q}_n \mathbf{Q}_m \rangle] \right. \right. \\ &\quad \left. \left. - \frac{n_p \zeta}{2} \left\{ \sum_{m,n} \left(\mathcal{C}_{mn} - \frac{1}{1 + 2\theta} \mathcal{S}_{mn} \right) [\langle \boldsymbol{\kappa} \cdot (\mathbf{Q}_m \mathbf{Q}_n) \rangle + \langle (\mathbf{Q}_m \mathbf{Q}_n) \cdot \boldsymbol{\kappa}^T \rangle] \right\} \right] \right] \end{aligned} \quad (89)$$

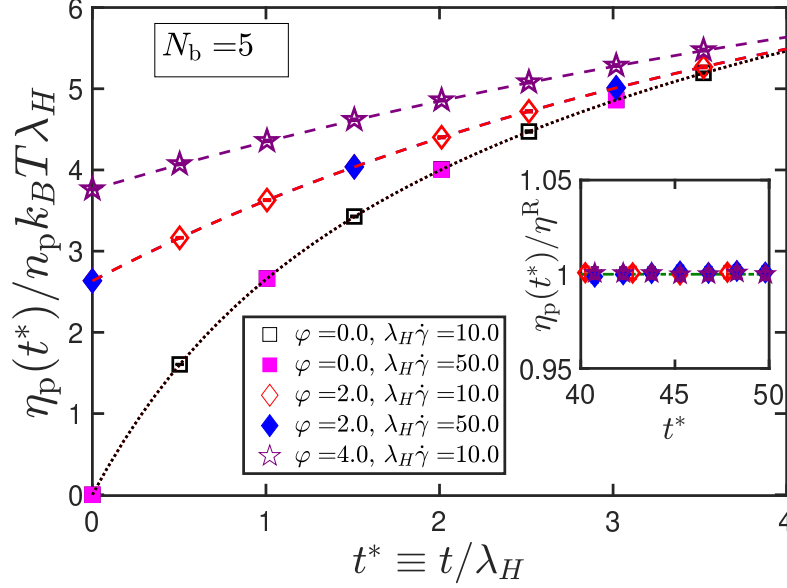


FIG. S5. Validating the expression for the transient evolution of shear viscosity for a five-bead Rouse chain with preaveraged internal friction for various values of the dimensionless shear rate ($\lambda_H \dot{\gamma}$) and internal friction parameter (φ). Lines represent Eq. (92) and symbols are BD simulations results. Inset shows the steady-state values of viscosity for the various cases.

where $\mathcal{L} = \mathbf{J} \cdot \mathcal{C}$ and $\mathcal{S} = \mathbf{\Lambda} \cdot \mathcal{C}$, with \mathcal{C} composed of \mathcal{C}_{jk} . The xy - component of the stress tensor is written as

$$\tau_{p,xy} = -n_p H \left[\left(\frac{1}{1+2\theta} \right) \sum_{m,n} \mathcal{L}_{mn} \langle \underline{Q_m^{(x)} Q_n^{(y)}} \rangle \right] - \frac{n_p \zeta \dot{\gamma}}{2} \left\{ \sum_{m,n} \left(\mathcal{C}_{mn} - \frac{1}{1+2\theta} \mathcal{S}_{mn} \right) \left[\langle \underline{Q_m^{(y)} Q_n^{(y)}} \rangle \right] \right\} \quad (90)$$

Following a procedure identical to that described in Sec. II B, the underlined terms are evaluated to be

$$\begin{aligned} \langle \underline{Q_m^{(x)} Q_n^{(y)}} \rangle &= \left(\frac{k_B T}{H} \right) (\lambda_H \dot{\gamma}) \sum_q \Pi_{mq} \Pi_{nq} I_q(t) \\ \langle \underline{Q_m^{(y)} Q_n^{(y)}} \rangle &= \left(\frac{k_B T}{H} \right) \delta_{mn} \end{aligned} \quad (91)$$

from which the expression for the dimensionless shear viscosity may be obtained as

$$\begin{aligned} \frac{\eta_p(t^*)}{n_p k_B T \lambda_H} &\equiv - \frac{\tau_{p,xy}}{n_p k_B T \lambda_H \dot{\gamma}} \\ &= \left(\frac{1}{1+2\theta} \right) \sum_{m,n,q} \Pi_{mq} \mathcal{L}_{mn} \Pi_{nq} I_q(t^*) + 2 \text{tr} \left[\mathbf{c} - \frac{1}{1+2\theta} \mathbf{S} \right] \end{aligned} \quad (92)$$

with

$$I_q(t^*) = 2 \left(\frac{\tilde{b}_q}{\tilde{a}_q} \right) \left\{ 1 - \exp \left[- \left(\frac{\tilde{a}_q}{1+2\theta} \right) \frac{t^*}{2} \right] \right\}, \quad (93)$$

In Fig. S5, the solution given by Eq. (92) is compared against BD simulation data for the preaveraged IV model, obtained by numerically integrating Eq. (68) and using the stress tensor expression given by Eq. (89), for a variety of internal friction parameters and shear rates. An excellent agreement is observed between the results obtained using the two approaches.

¹Khatrri, B. S. & McLeish, T. C. B. Rouse Model with Internal Friction: A Coarse Grained Framework for Single Biopolymer Dynamics. *Macromolecules* **40**, 6770–6777 (2007).

²Bird, R. B., Curtiss, C. F., Armstrong, R. C. & Hassager, O.

Dynamics of Polymeric Liquids - Volume 2 : Kinetic Theory (John Wiley and Sons, New York, 1987).

³Ottinger, H. C. *Stochastic Processes in Polymeric Fluids* (Springer, Berlin, 1996).

- ⁴Kailasham, R., Chakrabarti, R. & Prakash, J. R. Rouse model with fluctuating internal friction (2021). Preprint at <https://arxiv.org/abs/2102.09112>.
- ⁵Verdier, P. H. Monte carlo studies of lattice-model polymer chains. i. correlation functions in the statistical-bead model. *J. Chem. Phys.* **45**, 2118–2121 (1966).
- ⁶Kopf, A., Dünweg, B. & Paul, W. Dynamics of polymer "isotope" mixtures: Molecular dynamics simulation and Rouse model analysis. *J. Chem. Phys.* **107**, 6945–6955 (1997).
- ⁷Doi, M. & Edwards, S. F. *The Theory of Polymer Dynamics* (Clarendon, Oxford, 1986).
- ⁸Howard, M. P. & Milner, S. T. Numerical simulation methods for the Rouse model in flow. *Phys. Rev. E* **84**, 051804 (2011).
- ⁹Oldham, K. B. & Spanier, J. *Chapter 2: Differentiation and Integration to Integer Order*, vol. 111 of *Mathematics in Science and Engineering* (Elsevier, 1974).
- ¹⁰Bhattacharyya, P. & Cherayil, B. J. Chain extension of a confined polymer in steady shear flow. *J. Chem. Phys.* **137** (2012).
- ¹¹Prakash, J. R. The kinetic theory of dilute solutions of flexible polymers: Hydrodynamic interaction. In Siginer, D. A., De Kee, D. & Chhabra, R. P. (eds.) *Rheology Series*, vol. 8, 467–517 (Elsevier, 1999).
- ¹²Manke, C. W. & Williams, M. C. Stress Jump at the Inception of Shear and Elongational Flows of Dilute Polymer Solutions, Due to Internal Viscosity. *J. Rheol.* **31**, 495–510 (1988).
- ¹³Dasbach, T. P., Manke, C. W. & Williams, M. C. Complex viscosity for the rigorous formulation of the multibead internal viscosity model with hydrodynamic interaction. *J. Phys. Chem.* **96**, 4118–4125 (1992).
- ¹⁴Schieber, J. D. & Öttinger, H. C. On consistency criteria for stress theory models tensors in kinetic. *J. Rheol.* **38**, 1909 (1994).